Supplementary information

β-PDGF Receptor Expressed by Hepatic Stellate Cells Regulates Fibrosis in Murine Liver Injury, but Not Carcinogenesis

Peri Kocabayoglu, Abigale Lade, Youngmin A. Lee, Ana-Cristina Dragomir, Xiaochen Sun, M. Isabel Fiel, Swan Thung, Costica Aloman, Philippe Soriano, Yujin Hoshida, Scott L. Friedman

[1] Division of Liver Diseases, Department of Medicine, Icahn School of Medicine at Mount Sinai, New York, NY, USA
[2] Department of General, Visceral and Transplant Surgery, University Hospital Essen, Germany
[3] Department of Pathology, Icahn School of Medicine at Mount Sinai, New York, NY, USA
[4] Current address: Division of Gastroenterology and Hepatology, Department of Medicine, University of Illinois at Chicago, Chicago, IL, USA
[5]Developmental and Regenerative Biology, Icahn School of Medicine at Mount Sinai, New York, NY
[6] Liver Cancer Program, Tisch Cancer Institute, Icahn School of Medicine at Mount Sinai, New York, NY

Table of Contents

Supplementary Methods

Common Bile Duct Ligation

BDL was performed on 8-week-old age-matched male mice. Animals were anesthetized using isoflurane (Forane, Baxter, Deerfield, IL), followed by midline laparotomy and ligation of the common bile duct with 4-0 silk ligatures. Sham-operated animals received laparotomy and blunt manipulation of the common bile duct without ligation. The peritoneum and skin were closed using monofilament synthetic absorbable sutures (PDS and Monocryl, respectively, Ethicon, Bridgewater, NJ). Mice were sacrificed 14 days after surgery.

Liver Tests

Quantitative determination of serum aspartate aminotransferase (AST) and alanine aminotransferase (ALT) levels was performed using spectrophotometer analysis (Pointe Scientific Inc., Canton, MI).

Western Blot

Whole liver samples were homogenized prior to centrifugation in lysis buffer complemented with protease inhibitor (Complete Lysis-M kit, Roche Diagnostics, Indianapolis, IN) and phosphatase inhibitor (Halt Phosphatase Inhibitor Single-Use Cocktail, Thermo Scientific, Waltham, MA). Cell extracts of cultured stellate cells were prepared by centrifuging the cells in lysis buffer with inhibitors. Protein concentration was determined using a Bio-Rad DC kit (Bio-Rad Laboratories, Hercules, CA). Cell and whole liver lysates were subjected to immunoblot analysis. Blots were developed using the ECL Detection System (Amersham Pharmacia Biotech, Buckinghamshire, England). Densitometric analysis of bands was performed with ImageJ software (rsbweb.nih.gov/ij, NIH, Bethesda, MD). Western blot membranes were incubated using the following primary antibodies: Rabbit anti-β-PDGFR (1:500) (Santa Cruz Biotechnology, Santa Cruz, CA), rabbit anti-phospho-β-PDGFR (1:500) (Santa Cruz Biotechnology, Santa Cruz, CA), rabbit anti-αSMA (1:500) (Millipore, Billerica, MA), rabbit anti-Collagen I (1:1,000) (Rockland Immunochemicals, Gilbertsville, PA), rabbit anti-Calnexin (1:3,000) (Abcam, Cambridge, England). The reactions were detected with a horseradish peroxidase–conjugated secondary antibody (Anti-rabbit IgG, Cell Signaling, Danvers, MA).

Quantification of Hydroxyproline Content

Hepatic hydroxyproline content was assayed and results expressed as μg/g of wet liver tissue. For each experimental group, liver samples of a total of n=5 animals were used. Photometrical determination of hepatic hydroxyproline content was performed in liver hydrolysates. Snap-frozen liver segments (50mg) were hydrolyzed in 6N HCl at 110°C for 16 h and filtered. Aliquots (50 μl) of each sample were incubated with chloramine T solution for 5 min following incubation in Ehrlich's reagent for 45 min at 50°C. Absorption for each sample was measured in a triplicate at 570 nm. Results are expressed as μg/g of wet liver tissue. For each experimental group, liver samples of a total of n=5 animals were used.

Reverse Transcription and Real-Time Quantitative PCR

RNA was extracted from liver tissue using Trizol (Life Technologies, Carlsbad, CA), followed by purification using Qiagen mini columns (Qiagen, Germantown, MD) with an on-column deoxyribonuclease treatment. One microgram of RNA was reverse-transcribed using RNA to cDNA EcoDry Premix (double Primed) Kit (Clontech, Mountain View, CA). IQ SYBR Green Supermix (Bio-Rad Laboratories, Hercules, CA) was used for quantitative PCR on the lightCycler480 System (Roche Diagnostics, Indianapolis, IN). Samples were analyzed in triplicate using Microsoft Excel software (Microsoft Corp., Redmond, WA). Data are represented as the relative expression of fibrogenic genes after normalizing to glyceraldehyde 3-phosphate dehydrogenase (GAPDH). (See Supplementary Table 1 for a complete list of primers.)

Flow Cytometry

Mice were injected three times with either corn oil or CCl_4 every 48 hours. 44 hours after the last injection mice received a single i.p. injection of BrdU (1.5mg/150μl PBS). Stellate cells were isolated 4 hours later. Cells were first stained for CD45 (APC-CD45-Cy7, eBioscience, San Diego, CA) to exclude contaminating inflammatory cells. Intracellular BrdU staining was performed after fixation and permeabilization of stellate cells following the manufacturer's protocol (BrdU Flow Kit, BD Biosciences, San Jose, CA). Multiparameter analyses of stained cell suspension were performed on an LSR II (BD) and analyzed with FlowJo software (Tree Star, Ashland, OR).

Bioinformatics and Statistical Analysis

Enrichment of molecular pathways was evaluated by Gene Set Enrichment Analysis (GSEA) [3] on a comprehensive gene set collection in Molecular Signatures Database

(www.broadinstitute.org/gsea/msigdb). The 186-gene human prognostic gene signature was reported in our previous study [1, 2]. β-PDGFR-knockout gene signature was defined as top and bottom differentially expressed genes (100 genes for each) between the Δβ-PDGFR and wild-type cells (3 biological replicates for each condition) by using random permutation t-test. Induction of β-PDGFR-knockout gene signature was assessed in genome-wide expression profiles of 216 patients with hepatitis-C-related, early-stage liver cirrhosis that were derived from our previous study [2] (GEO accession number: GSE15654). Genes in the dataset were rank-ordered according to Cox score calculated for association with HCC development. Enrichment of the gene signature was first assessed for each of the top and bottom genes separately by GSEA. Enrichment of the signature was also assessed for combination of the top and bottom genes as follows. Briefly, enrichment of each of the top or bottom genes associated with the clinical outcome were separately measured by using Kolmogorov–Smirnov statistic [3], and absolute values of the statistic for both gene sets were summed to calculate a combined gene set enrichment score (CES). Statistical significance of the CES was evaluated as a nominal p-value based on an empirical null distribution of the CES generated by randomly picking the same number of genes from the genome-wide profile and by recalculating the CES 1,000 times. All bioinformatics data analyses were performed by using analysis modules implemented in GenePattern software (www.genepatter.broadinstitute.org) and custom R codes (www.r-project.org). Multiple hypothesis testing was corrected by using false discovery rate (FDR), and FDR<0.05 was regarded as statistically significant.

Comparison of Pdgfrb knockout-mediated differential gene expression between DNA microarray and RT-qPCR was performed choosing five of the top differentially expressed genes (Anxa1, Dab2, Ergic2, Lpp, and Prdx5) between wild type and β-PDGFR-knockout mice as selected from DNA microarray data. Log-transformed (base 2) fold changes (wild type / β-PDGFR-knockout) were compared by Pearson correlation test.

Experimental results are represented as mean +/- SEM and were compared by Student's t-test. P-values of at least 3 independent determinations were calculated using Microsoft Excel software. $P < 0.05$ were considered statistically significant. Statistical significance was expressed as follows: * $P < 0.05$, ** $P < 0.01$. Graphs were created using Prism 6 software (GraphPad Software, Inc.).

Ingenuity Pathway Analysis

To identify molecular interaction networks between genes induced by β-PDGFR signaling, the top 100 up-regulated genes in wild-type mouse hepatic stellate cells in comparison to β-

PDGFR-knockout were subjected to Ingenuity Pathway Analysis (Supplementary Table 2, Supplementary Table 4, Supplementary Table 5).

Supplementary Results

β-PDGFR Expression accelerates fibrosis upon liver injury in a BDL model

To confirm that the findings were not restricted to a single model of liver injury, we analyzed mice only 14 days after common bile duct (BDL) or sham laparotomy; longer intervals led to dramatically reduced weight and poor feeding. Control mice had better survival rates than Δβ-PDGFR mice (data not shown). Both groups of mice displayed elevated fibrosis content (Supplementary Fig. 5 A, B). Although the differences in fibrosis between both groups did not reach statistical significance, Δβ-PDGFR mice showed less fibrosis by Sirius Red morphometry and liver injury as assessed by serum transaminase levels (Supplementary Fig. 5 B, C) than β-PDGFR wild type mice.

Deregulated Molecular Pathways Downstream of β-PDGF Signaling in Primary Mouse Hepatic Stellate Cells

We performed genome-wide expression profiling of primary stellate cells isolated from β-PDGFR$^{fl/fl}$ GFAP-Cre negative (β-PDGFR) and β-PDGFR$^{fl/fl}$ GFAP-Cre positive (Δβ-PDGFR) mice that were either treated with 10ng/ml PDGF-B over 6 hours or left untreated. Molecular pathway analysis using gene set enrichment analysis (GSEA) revealed enrichment of genes that were related to ERK and AKT signal transduction and the NF-kB signaling pathway (for a comprehensive summary of GSEA see Supplementary Table 3). *Ingenuity* pathway analysis confirmed this correlation. Comparison of the β-PDGFR with the Δβ-PDGFR array signature showed a high correlation of ERK and AKT pathway mediators when cells were either left untreated (Supplementary Fig. 11A) or treated (Supplementary Fig. 11B) with the ligand.

Further analysis revealed novel pathway correlations with the β-PDGFR signature (Supplementary Fig. 12). GSEA showed enrichment of genes classified in the IL1R pathway even when cells were untreated (Supplementary Fig. 12A). This enrichment revealed a stronger correlation when cells had been exposed to PDGF-B (Supplementary Fig. 12B). The same correlations were seen for the NF-kB pathway gene set. This gene enrichment positively correlated with the β-PDGFR phenotype, and showed a negative correlation with the knockout-phenotype when cells were left untreated (Supplementary Fig. 12C) or treated with PDGF-B (Supplementary Fig. 12D). Ingenuity pathway analysis confirmed these findings (Supplementary Fig. 12E, F). A comprehensive pathway analysis for the comparison of the β-

PDGFR versus Δβ-PDGFR signature without ligand is summarized in Supplementary Table 4, and a comparison between the β-PDGFR and Δβ-PDGFR signature with ligand in Supplementary Table 5.

References

[1] Hoshida Y, Villanueva A, Kobayashi M, Peix J, Chiang DY, Camargo A, et al. Gene expression in fixed tissues and outcome in hepatocellular carcinoma. N Engl J Med 2008;359(19): 1995-2004.

[2] Hoshida Y, Villanueva A, Sangiovanni A, Sole M, Hur C, Andersson KL, et al. Prognostic gene expression signature for patients with hepatitis C-related early-stage cirrhosis. Gastroenterology 2013;144(5): 1024-1030.

[3] Subramanian A, Tamayo P, Mootha VK, Mukherjee S, Ebert BL, Gillette MA, et al. Gene set enrichment analysis: a knowledge-based approach for interpreting genome-wide expression profiles. Proc Natl Acad Sci U S A 2005;102(43): 15545-15550.

Supplementary Table 1. List of Primers

Name	Sequence
mβ-PDGFR F	5'-ACTACATCTCCAAAGGCAGCACCT-3'
mβ-PDGFR R	5'-TGTAGAACTGGTCGTTCATGGGCA-3'
mCollagenα1(I) F	5'-GTCCCTGAAGTCAGCTGCATA-3'
mCollagenα1(I) R	5'-TGGGACAGTCCAGTTCTTCAT-3'
mαSMA F	5'-TCCTCCCTGGAGAAGAGCTAC-3'
mαSMA R	5'-TATGGTGGTTTCGTGGATGC-3'
mAnxa1 F	5'-TGCCGAGAAGCTGTACGAAGC-3
mAnxa1 R	5'-CCACCACACAGAGCCACCAG-3'
mDab2 F	5'-CGAACCCTTTTGTGGGAAGC-3'
mDab2 R	5'-GGGGACATCTGGCCTGGAG-3'
mLpp F	5'-TACCTGGAAGCGGGAAGCTG-3'
mLpp R	5'-TCTTCTGGGCGGAATGATGG-3'
mPrdx5_1 F	5'-TGGAGTCCCTGGGGCATTTA-3'
mPrdx5_1 R	5'-AGGAGCCGAACCTTGCCTTC-3'
mPrdx5_2 F	5'-GCCTGGGTTTGTGGAGCAAG-3'
mPrdx5_2 R	5'-GCCGACGATTCCCAAAGAGA-3'
mErgic2_1 F	5'-CAACTGCACTGCCACCAAGG-3'
mErgic2_1 R	5'-CCCGGAACAAGCTCTCCAAA-3'
mErgic2_2 F	5'-CCCAGCAGAGAGAGTGGCAGA-3'
mErgic2_2 R	5'-GGATTGCCTTGCCCACAGTT-3'
mGAPDH F	5'-CAATGACCCCTTCATTGACC-3'
mGAPDH R	5'-GATCTCGCTCCTGGAAGATG-3'

Supplementary table 2

Ingenuity pathway analysis for enriched 186-gene signature genes in Pdgfrb-wildt ype hepatic stellate cells compared to knockout without Pdgfb treatment.

Analysis Name: 186gene_core_enrichment_genes_on_woPdgfb_only_poor - 2013-11-15 07:49 AM
Analysis Creation Date: 2013-11-15
Build version: 242990
Content version: 17199142 (Release Date: 2013-09-17)

Analysis settings

View

Reference set: Ingenuity Knowledge Base (Genes Only)
Relationship to include: Direct and Indirect
Includes Endogenous Chemicals
Optional Analyses: My Pathways My List

Filter Summary:
Consider only relationships where
confidence = Experimentally Observed
Cutoff:

Top Networks

ID	Associated Network Functions	Score
1	Cell Death and Survival, Tumor Morphology, Cellular Movement	33
2	Cell Cycle, Cellular Response to Therapeutics, Molecular Transport	8

Top Diseases and Bio Functions

Diseases and Disorders

Name	p-value	# Molecules
Cancer	1.16E-05 - 1.20E-02	15
Hematological Disease	1.16E-05 - 1.18E-02	8
Reproductive System Disease	6.13E-05 - 1.20E-02	11
Immunological Disease	8.30E-05 - 1.12E-02	6
Organismal Injury and Abnormalities	1.45E-04 - 7.75E-03	6

Molecular and Cellular Functions

Name	p-value	# Molecules
Cellular Movement	2.06E-06 - 1.20E-02	11
Cell Death and Survival	6.76E-06 - 1.20E-02	10
Cell-To-Cell Signaling and Interaction	8.99E-05 - 1.12E-02	7
Gene Expression	1.06E-04 - 1.06E-04	3
Cellular Compromise	1.90E-04 - 1.20E-02	4

Physiological System Development and Function

Name	p-value	# Molecules
Tumor Morphology	6.95E-06 - 1.12E-02	4
Hematological System Development and Function	1.03E-05 - 1.20E-02	8
Immune Cell Trafficking	1.03E-05 - 1.16E-02	6
Tissue Development	8.99E-05 - 1.12E-02	8
Lymphoid Tissue Structure and Development	3.19E-04 - 1.20E-02	2

Top Canonical Pathways

Name	p-value	Ratio
Death Receptor Signaling	1.12E-03	2/68 (0.029)
Induction of Apoptosis by HIV1	1.16E-03	2/67 (0.03)
IL-15 Signaling	1.24E-03	2/72 (0.028)
Small Cell Lung Cancer Signaling	1.67E-03	2/94 (0.021)
PEDF Signaling	1.67E-03	2/79 (0.025)

Top Molecules

Other up-regulated

Molecules	Exp. Value	Exp. Chart
DAB2	↑1.351	
LPP	↑1.283	
ANXA1	↑1.278	
NFKB2	↑0.957	
EPM2AIP1	↑0.900	
SERPINB2	↑0.899	
ITGA9	↑0.826	
IQGAP1	↑0.809	
IER3	↑0.739	
CCDC6	↑0.541	

Other down-regulated

Molecules	Exp. Value	Exp. Chart

Top Upstream Regulators

Upstream Regulator	p-value of overlap	Predicted Activation State
butyric acid	7.64E-09	
AGT	9.96E-09	Activated
TP53	3.87E-08	
HRAS	1.71E-06	
SB203580	3.20E-06	Inhibited

Top My Lists

Name	p-value	Ratio

Top My Pathways

Name	p-value	Ratio

Top Tox Lists

Name	p-value	Ratio
Acute Renal Failure Panel (Rat)	1.28E-03	2/62 (0.032)
Increases Liver Hyperplasia/Hyperproliferation	1.36E-03	2/64 (0.031)
Decreases Permeability Transition of Mitochondria and Mitochondrial Membrane	6.03E-03	1/7 (0.143)
Primary Glomerulonephritis Biomarker Panel (Human)	9.46E-03	1/11 (0.091)
Recovery from Ischemic Acute Renal Failure (Rat)	1.2E-02	1/14 (0.071)

Top Tox Functions

Cardiotoxicity

Name	p-value	# Molecules
Cardiac Inflammation	2.59E-03 - 2.59E-03	1
Cardiac Hypertrophy	1.92E-02 - 1.04E-01	2
Cardiac Necrosis/Cell Death	2.22E-02 - 2.39E-02	2
Cardiac Damage	3.48E-02 - 3.48E-02	1

Hepatotoxicity

Name	p-value	# Molecules
Hepatocellular Carcinoma	1.20E-03 - 4.23E-02	3
Liver Hyperplasia/Hyperproliferation	1.20E-03 - 4.23E-02	4
Liver Necrosis/Cell Death	1.35E-02 - 1.09E-01	2
Liver Proliferation	1.26E-01 - 1.26E-01	1

Nephrotoxicity

Name	p-value	# Molecules
Renal Hypertrophy	4.31E-03 - 1.97E-02	1
Renal Inflammation	4.31E-03 - 1.77E-01	2
Renal Nephritis	4.31E-03 - 1.77E-01	2
Renal Necrosis/Cell Death	8.60E-03 - 5.63E-02	2
Renal Degeneration	1.29E-02 - 1.29E-02	1

Network 1 : 186gene_core_enrichment_genes_on_woPdgfb_only_poor - 2013-11-15 07:49 AM : 186gene_core_enrichment_genes_on_woPdgfb_only_poor : 186gene_core_enrichment_genes_on_woPdgfb_only_poor - 2013-11-15 07:49 AM

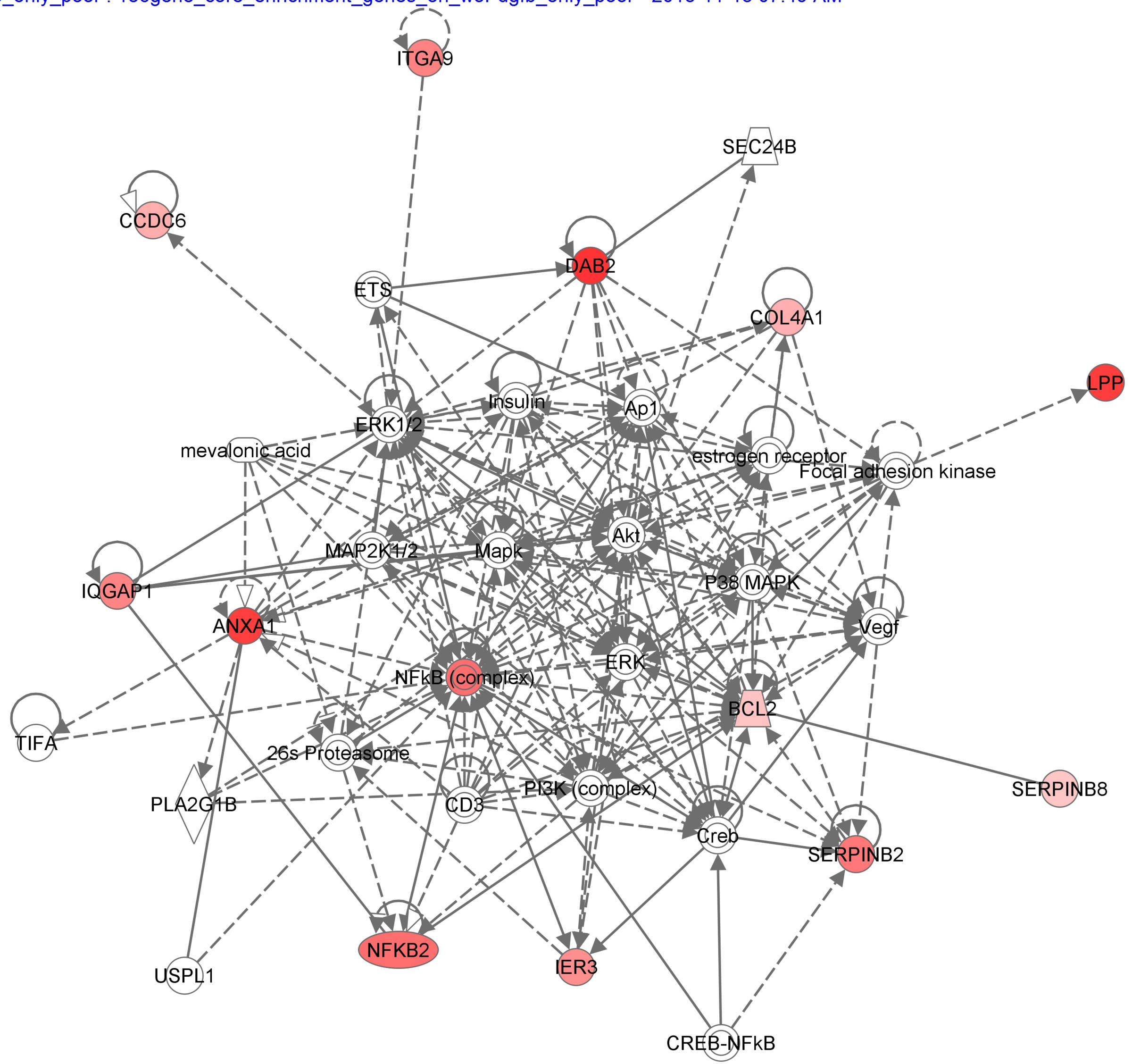

Network 2 : 186gene_core_enrichment_genes_on_woPdgfb_only_poor - 2013-11-15 07:49 AM : 186gene_core_enrichment_gene
on_woPdgfb_only_poor : 186gene_core_enrichment_genes_on_woPdgfb_only_poor - 2013-11-15 07:49 AM

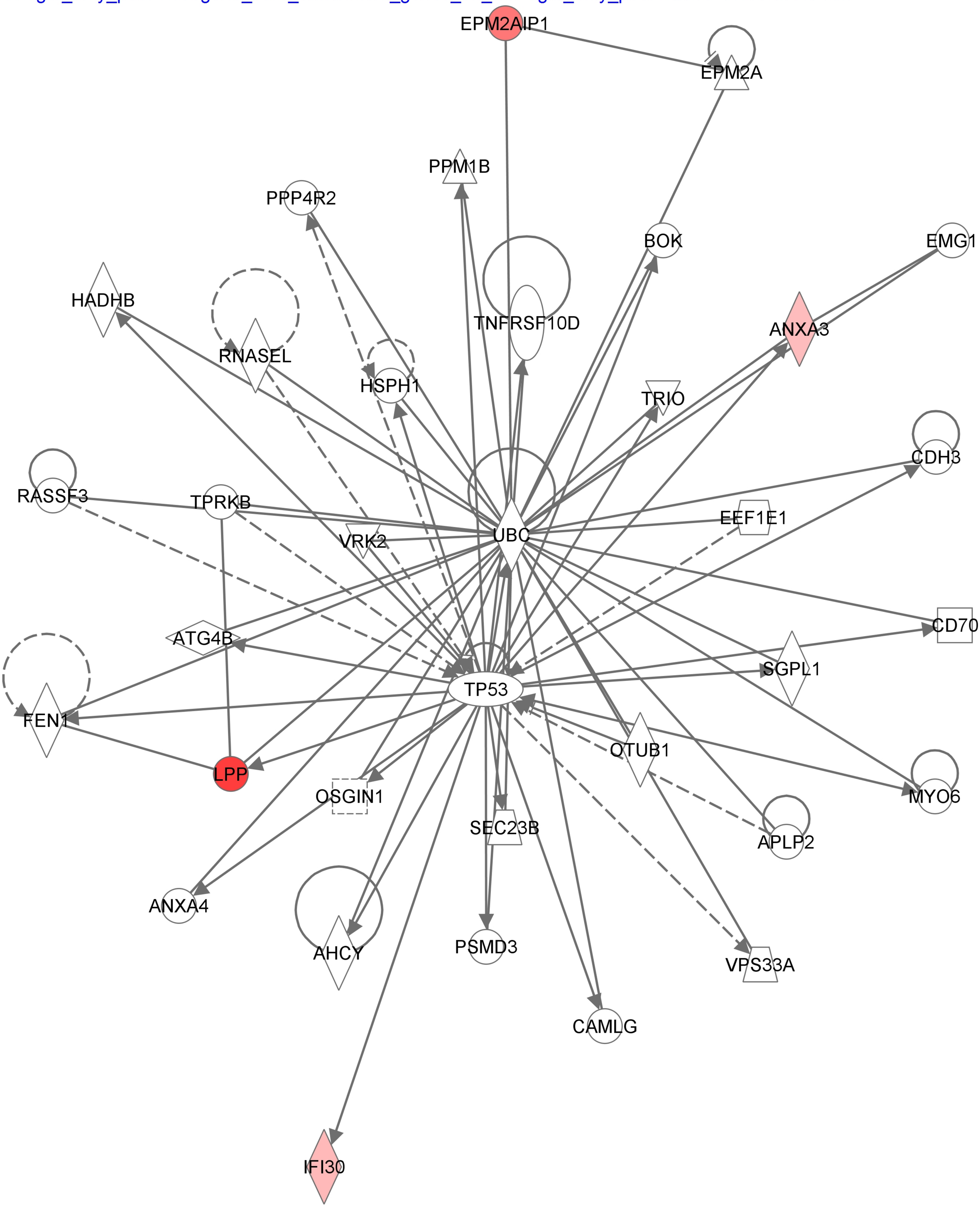

Supplementary Table 3

Gene sets associated with Pdgfrb knockout in mouse hepatic stellate cells (Gene Set Enrichment Analysis)

Gene sets with FDR <0.25, top five (when FDR ≥0.25), or top 20 (when FDR <0.25) are shown. FDR ≥ 0.25 are shaded with gray.
NES: normalized enrichment score, FDR: false discovery rate, Click each gene set name for detailed information.

Isolated hepatic stellate cells (no treatment)

Gene set database	Enriched in	Gene set	NES	p-value	FDR
Biocarta	Wild-Type	BIOCARTA_NTHI_PATHWAY	0.620	3.320	0.000
(Curated pathway database)		BIOCARTA_IL1R_PATHWAY	0.500	3.130	0.000
		BIOCARTA_KERATINOCYTE_PATHWAY	0.360	2.650	0.000
		BIOCARTA_HCMV_PATHWAY	0.520	2.520	0.000
		BIOCARTA_TOLL_PATHWAY	0.380	2.510	0.000
		BIOCARTA_NFKB_PATHWAY	0.460	2.470	0.000
		BIOCARTA_RHO_PATHWAY	0.380	2.430	0.000
		BIOCARTA_GCR_PATHWAY	0.460	2.300	0.000
		BIOCARTA_FMLP_PATHWAY	0.340	2.280	0.000
		BIOCARTA_LAIR_PATHWAY	0.470	2.190	0.002
		BIOCARTA_NFAT_PATHWAY	0.280	2.150	0.005
		BIOCARTA_RAC1_PATHWAY	0.380	2.140	0.000
		BIOCARTA_IL10_PATHWAY	0.440	2.140	0.000
		BIOCARTA_MAPK_PATHWAY	0.210	2.140	0.003
		BIOCARTA_VIP_PATHWAY	0.390	2.130	0.000
		BIOCARTA_CTCF_PATHWAY	0.410	2.120	0.005
		BIOCARTA_CD40_PATHWAY	0.470	2.080	0.003
		BIOCARTA_EIF4_PATHWAY	0.380	2.070	0.000
		BIOCARTA_TGFB_PATHWAY	0.420	2.050	0.005
		BIOCARTA_HIVNEF_PATHWAY	0.260	2.040	0.005
	Knockout	BIOCARTA_P53_PATHWAY	-0.350	-1.740	0.021
		BIOCARTA_CELLCYCLE_PATHWAY	-0.310	-1.720	0.017
		BIOCARTA_RACCYCD_PATHWAY	-0.260	-1.630	0.041
		BIOCARTA_CARM_ER_PATHWAY	-0.220	-1.540	0.052
		BIOCARTA_ACH_PATHWAY	-0.260	-1.250	0.189
Kyoto Encyclopedia of Genes and Genomes (KEGG)	Wild-Type	KEGG_LEISHMANIA_INFECTION	4.020	0.000	0.000
(Curated pathway database)		KEGG_LYSOSOME	3.110	0.000	0.001
		KEGG_OLFACTORY_TRANSDUCTION	2.950	0.000	0.000
		KEGG_TOLL_LIKE_RECEPTOR_SIGNALING_PATHWAY	2.760	0.000	0.001
		KEGG_GRAFT_VERSUS_HOST_DISEASE	2.700	0.000	0.000
		KEGG_APOPTOSIS	2.660	0.000	0.001
		KEGG_REGULATION_OF_ACTIN_CYTOSKELETON	2.650	0.000	0.000
		KEGG_ANTIGEN_PROCESSING_AND_PRESENTATION	2.600	0.000	0.001
		KEGG_PATHOGENIC_ESCHERICHIA_COLI_INFECTION	2.600	0.000	0.001
		KEGG_INTESTINAL_IMMUNE_NETWORK_FOR_IGA_PRODUCTION	2.560	0.000	0.001
		KEGG_NOD_LIKE_RECEPTOR_SIGNALING_PATHWAY	2.520	0.000	0.001
		KEGG_FC_GAMMA_R_MEDIATED_PHAGOCYTOSIS	2.420	0.000	0.002
		KEGG_B_CELL_RECEPTOR_SIGNALING_PATHWAY	2.390	0.001	0.003
		KEGG_ADIPOCYTOKINE_SIGNALING_PATHWAY	2.380	0.000	0.003
		KEGG_PANCREATIC_CANCER	2.360	0.000	0.003
		KEGG_NEUROTROPHIN_SIGNALING_PATHWAY	2.300	0.000	0.005
		KEGG_PATHWAYS_IN_CANCER	2.290	0.001	0.005
		KEGG_RENAL_CELL_CARCINOMA	2.250	0.003	0.007
		KEGG_VALINE_LEUCINE_AND_ISOLEUCINE_DEGRADATION	2.240	0.002	0.007
		KEGG_VIRAL_MYOCARDITIS	2.240	0.000	0.007
	Knockout	KEGG_RIBOSOME	-4.200	0.000	0.000
		KEGG_OXIDATIVE_PHOSPHORYLATION	-3.550	0.000	0.000
		KEGG_PARKINSONS_DISEASE	-2.980	0.000	0.000
		KEGG_DNA_REPLICATION	-2.720	0.000	0.000
		KEGG_HUNTINGTONS_DISEASE	-2.690	0.000	0.000

Gene sets associated with Pdgfrb knockout in mouse hepatic stellate cells (Gene Set Enrichment Analysis)

Gene sets with FDR <0.25, top five (when FDR ≥0.25), or top 20 (when FDR <0.25) are shown. FDR ≥ 0.25 are shaded with gray.
NES: normalized enrichment score, FDR: false discovery rate, Click each gene set name for detailed information.

Isolated hepatic stellate cells (with treatment)

Gene set database	Enriched in	Gene set	NES	p-value	FDR
Biocarta	Wild-Type	BIOCARTA_IL1R_PATHWAY	3.300	0.000	0.000
(Curated pathway database)		BIOCARTA_NFKB_PATHWAY	2.880	0.000	0.001
		BIOCARTA_LAIR_PATHWAY	2.660	0.000	0.001
		BIOCARTA_NTHI_PATHWAY	2.540	0.000	0.001
		BIOCARTA_TOLL_PATHWAY	2.530	0.000	0.001
		BIOCARTA_ERYTH_PATHWAY	2.160	0.003	0.028
		BIOCARTA_CDMAC_PATHWAY	2.140	0.002	0.027
		BIOCARTA_KERATINOCYTE_PATHWAY	2.140	0.000	0.025
		BIOCARTA_CD40_PATHWAY	2.110	0.003	0.027
		BIOCARTA_NKT_PATHWAY	2.070	0.002	0.030
		BIOCARTA_INFLAM_PATHWAY	2.040	0.005	0.030
		BIOCARTA_RELA_PATHWAY	1.990	0.007	0.041
		BIOCARTA_CHREBP2_PATHWAY	1.980	0.006	0.041
		BIOCARTA_TGFB_PATHWAY	1.910	0.012	0.058
		BIOCARTA_IL10_PATHWAY	1.890	0.005	0.060
		BIOCARTA_CERAMIDE_PATHWAY	1.790	0.013	0.101
		BIOCARTA_AKT_PATHWAY	1.740	0.026	0.123
		BIOCARTA_TNFR2_PATHWAY	1.730	0.019	0.121
		BIOCARTA_DC_PATHWAY	1.700	0.026	0.138
		BIOCARTA_COMP_PATHWAY	1.700	0.027	0.134
	Knockout	BIOCARTA_IGF1_PATHWAY	-1.770	0.015	0.813
		BIOCARTA_P53_PATHWAY	-1.710	0.021	0.553
		BIOCARTA_TFF_PATHWAY	-1.700	0.022	0.386
		BIOCARTA_INSULIN_PATHWAY	-1.590	0.049	0.503
		BIOCARTA_TPO_PATHWAY	-1.550	0.058	0.477
Kyoto Encyclopedia of Genes and Genomes (KEGG)	Wild-Type	KEGG_LEISHMANIA_INFECTION	4.110	0.000	0.000
(Curated pathway database)		KEGG_OLFACTORY_TRANSDUCTION	3.430	0.000	0.000
		KEGG_OXIDATIVE_PHOSPHORYLATION	2.880	0.000	0.000
		KEGG_TOLL_LIKE_RECEPTOR_SIGNALING_PATHWAY	2.830	0.000	0.000
		KEGG_NEUROACTIVE_LIGAND_RECEPTOR_INTERACTION	2.690	0.000	0.001
		KEGG_GRAFT_VERSUS_HOST_DISEASE	2.640	0.000	0.001
		KEGG_NOD_LIKE_RECEPTOR_SIGNALING_PATHWAY	2.540	0.000	0.001
		KEGG_RIG_I_LIKE_RECEPTOR_SIGNALING_PATHWAY	2.530	0.000	0.001
		KEGG_HEMATOPOIETIC_CELL_LINEAGE	2.490	0.000	0.001
		KEGG_TYPE_I_DIABETES_MELLITUS	2.400	0.000	0.003
		KEGG_APOPTOSIS	2.230	0.000	0.013
		KEGG_PARKINSONS_DISEASE	2.220	0.000	0.012
		KEGG_SYSTEMIC_LUPUS_ERYTHEMATOSUS	2.210	0.001	0.012
		KEGG_ALLOGRAFT_REJECTION	2.160	0.002	0.015
		KEGG_FOCAL_ADHESION	2.160	0.003	0.015
		KEGG_PEROXISOME	2.120	0.003	0.018
		KEGG_LYSOSOME	2.110	0.000	0.018
		KEGG_PRIMARY_IMMUNODEFICIENCY	2.050	0.000	0.026
		KEGG_CITRATE_CYCLE_TCA_CYCLE	2.030	0.002	0.028
		KEGG_CHEMOKINE_SIGNALING_PATHWAY	2.030	0.004	0.027
	Knockout	KEGG_PYRIMIDINE_METABOLISM	-2.390	0.000	0.018
		KEGG_SNARE_INTERACTIONS_IN_VESICULAR_TRANSPORT	-2.350	0.000	0.012
		KEGG_P53_SIGNALING_PATHWAY	-2.300	0.003	0.012
		KEGG_PROTEIN_EXPORT	-2.250	0.000	0.012
		KEGG_TIGHT_JUNCTION	-1.860	0.016	0.106
		KEGG_DNA_REPLICATION	-1.840	0.006	0.097
		KEGG_SPLICEOSOME	-1.790	0.003	0.107
		KEGG_CELL_CYCLE	-1.780	0.016	0.095
		KEGG_NUCLEOTIDE_EXCISION_REPAIR	-1.610	0.051	0.202
		KEGG_BASAL_CELL_CARCINOMA	-1.610	0.045	0.187
		KEGG_ALPHA_LINOLENIC_ACID_METABOLISM	-1.600	0.056	0.176
		KEGG_PURINE_METABOLISM	-1.590	0.034	0.172
		KEGG_OOCYTE_MEIOSIS	-1.530	0.050	0.205
		KEGG_ONE_CARBON_POOL_BY_FOLATE	-1.530	0.061	0.192
		KEGG_BASE_EXCISION_REPAIR	-1.490	0.072	0.212
		KEGG_BASAL_TRANSCRIPTION_FACTORS	-1.470	0.075	0.216
		KEGG_RNA_POLYMERASE	-1.460	0.074	0.212
		KEGG_FRUCTOSE_AND_MANNOSE_METABOLISM	-1.460	0.080	0.202
		KEGG_AMINOACYL_TRNA_BIOSYNTHESIS	-1.410	0.108	0.235

Reactome	Wild-Type	REACTOME_RESPONSE_TO_ELEVATED_PLATELET_CYTOSOLIC_CA2	3.730	0.000	0.000	Reactome	Wild-Type	REACTOME_OLFACTORY_SIGNALING_PATHWAY	3.460	0.000	0.000
(Curated pathway database)		REACTOME_INNATE_IMMUNE_SYSTEM	3.510	0.000	0.000	(Curated pathway database)		REACTOME_CHOLESTEROL_BIOSYNTHESIS	3.400	0.000	0.000
		REACTOME_TOLL_RECEPTOR_CASCADES	3.510	0.000	0.000			REACTOME_TCA_CYCLE_AND_RESPIRATORY_ELECTRON_TRANSPORT	3.020	0.000	0.000
		REACTOME_ACTIVATED_TLR4_SIGNALLING	3.500	0.000	0.000			REACTOME_CELL_SURFACE_INTERACTIONS_AT_THE_VASCULAR_WALL	3.000	0.000	0.000
		REACTOME_CYTOKINE_SIGNALING_IN_IMMUNE_SYSTEM	3.440	0.000	0.000			REACTOME_HEMOSTASIS	2.930	0.000	0.000
		REACTOME_MYD88_MAL_CASCADE_INITIATED_ON_PLASMA_MEMBRANE	3.410	0.000	0.000			REACTOME_RESPIRATORY_ELECTRON_TRANSPORT_ATP_SYNTHESIS_BY_CHEMIOSMOTIC_COUPLING_AND_HEAT_PRODUCTION_BY_UNCOUPLING_PROTEINS	2.870	0.000	0.000
		REACTOME_ADAPTIVE_IMMUNE_SYSTEM	3.370	0.000	0.000			REACTOME_ADAPTIVE_IMMUNE_SYSTEM	2.790	0.000	0.001
		REACTOME_CHOLESTEROL_BIOSYNTHESIS	3.190	0.000	0.000			REACTOME_INNATE_IMMUNE_SYSTEM	2.780	0.000	0.000
		REACTOME_TRAF6_MEDIATED_INDUCTION_OF_NFKB_AND_MAP_KINASES_UPON_TLR7_8_OR_9_ACTIVATION	3.150	0.000	0.000			REACTOME_CLASS_A1_RHODOPSIN_LIKE_RECEPTORS	2.660	0.000	0.001
		REACTOME_NFKB_AND_MAP_KINASES_ACTIVATION_MEDIATED_BY_TLR4_SIGNALING_REPERTOIRE	3.090	0.000	0.000			REACTOME_RIG_I_MDA5_MEDIATED_INDUCTION_OF_IFN_ALPHA_BETA_PATHWAYS	2.660	0.000	0.001
		REACTOME_TRANS_GOLGI_NETWORK_VESICLE_BUDDING	3.010	0.000	0.000			REACTOME_METABOLISM_OF_LIPIDS_AND_LIPOPROTEINS	2.630	0.000	0.001
		REACTOME_OLFACTORY_SIGNALING_PATHWAY	2.990	0.000	0.000			REACTOME_CYTOKINE_SIGNALING_IN_IMMUNE_SYSTEM	2.540	0.000	0.003
		REACTOME_FORMATION_OF_TUBULIN_FOLDING_INTERMEDIATES_BY_CCT_TRIC	2.810	0.000	0.000			REACTOME_SIGNALING_BY_ILS	2.520	0.000	0.003
		REACTOME_HEMOSTASIS	2.770	0.000	0.000			REACTOME_TOLL_RECEPTOR_CASCADES	2.450	0.001	0.004
		REACTOME_TRIF_MEDIATED_TLR3_SIGNALING	2.760	0.000	0.000			REACTOME_PLATELET_ACTIVATION_SIGNALING_AND_AGGREGATION	2.420	0.000	0.005
		REACTOME_NUCLEOTIDE_BINDING_DOMAIN_LEUCINE_RICH_REPEAT_CONTAINING_RECEPTOR_NLR_SIGNALING_PATHWAYS	2.750	0.000	0.000			REACTOME_RESPIRATORY_ELECTRON_TRANSPORT	2.410	0.000	0.005
		REACTOME_CLASS_I_MHC_MEDIATED_ANTIGEN_PROCESSING_PRESENTATION	2.680	0.000	0.001			REACTOME_TCR_SIGNALING	2.300	0.000	0.010
		REACTOME_PLATELET_ACTIVATION_SIGNALING_AND_AGGREGATION	2.590	0.000	0.001			REACTOME_GPCR_LIGAND_BINDING	2.300	0.000	0.009
		REACTOME_METABOLISM_OF_LIPIDS_AND_LIPOPROTEINS	2.570	0.000	0.001			REACTOME_RESPONSE_TO_ELEVATED_PLATELET_CYTOSOLIC_CA2	2.280	0.000	0.010
		REACTOME_GOLGI_ASSOCIATED_VESICLE_BIOGENESIS	2.560	0.000	0.001			REACTOME_INTERFERON_GAMMA_SIGNALING	2.270	0.002	0.011
	Knockout	REACTOME_CELL_CYCLE	-0.200	-4.480	0.000		Knockout	REACTOME_ACTIVATION_OF_CHAPERONE_GENES_BY_XBP1S	-3.480	0.000	0.000
		REACTOME_INFLUENZA_VIRAL_RNA_TRANSCRIPTION_AND_REPLICATION	-0.400	-4.450	0.000			REACTOME_CELL_CYCLE	-3.420	0.000	0.000
		REACTOME_DNA_REPLICATION	-0.260	-4.190	0.000			REACTOME_DEPOSITION_OF_NEW_CENPA_CONTAINING_NUCLEOSOMES_AT_THE_CENTROMERE	-3.120	0.000	0.000
		REACTOME_SRP_DEPENDENT_COTRANSLATIONAL_PROTEIN_TARGETING_TO_MEMBRANE	-0.370	-4.180	0.000			REACTOME_RNA_POL_I_PROMOTER_OPENING	-3.030	0.000	0.000
		REACTOME_TRANSLATION	-0.300	-4.150	0.000			REACTOME_UNFOLDED_PROTEIN_RESPONSE	-2.960	0.000	0.000
		REACTOME_PEPTIDE_CHAIN_ELONGATION	-0.400	-4.020	0.000			REACTOME_CELL_CYCLE_MITOTIC	-2.880	0.000	0.000
		REACTOME_CELL_CYCLE_MITOTIC	-0.190	-4.000	0.000			REACTOME_MRNA_SPLICING_MINOR_PATHWAY	-2.550	0.000	0.004
		REACTOME_NONSENSE_MEDIATED_DECAY_ENHANCED_BY_THE_EXON_JUNCTION_COMPLEX	-0.340	-3.920	0.000			REACTOME_RNA_POL_I_TRANSCRIPTION	-2.530	0.000	0.004
		REACTOME_MITOTIC_M_M_G1_PHASES	-0.250	-3.880	0.000			REACTOME_AMYLOIDS	-2.490	0.000	0.004
		REACTOME_DEPOSITION_OF_NEW_CENPA_CONTAINING_NUCLEOSOMES_AT_THE_CENTROMERE	-0.450	-3.810	0.000			REACTOME_MITOTIC_PROMETAPHASE	-2.480	0.000	0.004
		REACTOME_RESPIRATORY_ELECTRON_TRANSPORT	-0.400	-3.810	0.000			REACTOME_CHROMOSOME_MAINTENANCE	-2.460	0.000	0.005
		REACTOME_RESPIRATORY_ELECTRON_TRANSPORT_ATP_SYNTHESIS_BY_CHEMIOSMOTIC_COUPLING_AND_HEAT_PRODUCTION_BY_UNCOUPLING_PROTEINS	-0.340	-3.750	0.000			REACTOME_TELOMERE_MAINTENANCE	-2.440	0.000	0.005
		REACTOME_3_UTR_MEDIATED_TRANSLATIONAL_REGULATION	-0.330	-3.730	0.000			REACTOME_RNA_POL_I_RNA_POL_III_AND_MITOCHONDRIAL_TRANSCRIPTION	-2.270	0.000	0.014
		REACTOME_CHROMOSOME_MAINTENANCE	-0.300	-3.730	0.000			REACTOME_TRANSLATION	-2.250	0.007	0.014
		REACTOME_METABOLISM_OF_RNA	-0.190	-3.680	0.000			REACTOME_MEIOTIC_RECOMBINATION	-2.190	0.003	0.021
		REACTOME_RNA_POL_I_PROMOTER_OPENING	-0.440	-3.600	0.000			REACTOME_TRANSCRIPTION	-2.170	0.000	0.021
		REACTOME_TELOMERE_MAINTENANCE	-0.360	-3.530	0.000			REACTOME_PROCESSING_OF_CAPPED_INTRON_CONTAINING_PRE_MRNA	-2.160	0.000	0.021
		REACTOME_INFLUENZA_LIFE_CYCLE	-0.280	-3.510	0.000			REACTOME_DIABETES_PATHWAYS	-2.140	0.000	0.022
		REACTOME_METABOLISM_OF_MRNA	-0.200	-3.440	0.000			REACTOME_MEIOTIC_SYNAPSIS	-2.130	0.000	0.022
		REACTOME_MITOTIC_PROMETAPHASE	-0.290	-3.230	0.000			REACTOME_MITOTIC_M_M_G1_PHASES	-2.130	0.000	0.021
Gene Ontology	Wild-Type	IMMUNE_RESPONSE	3.200	0.000	0.000	Gene Ontology	Wild-Type	IMMUNE_RESPONSE	3.010	0.000	0.001
- Biological process		IMMUNE_SYSTEM_PROCESS	3.000	0.000	0.001	- Biological process		IMMUNE_SYSTEM_PROCESS	2.730	0.000	0.004
		NEGATIVE_REGULATION_OF_APOPTOSIS	2.710	0.000	0.003			PROTEIN_KINASE_CASCADE	2.330	0.000	0.059
		NEGATIVE_REGULATION_OF_PROGRAMMED_CELL_DEATH	2.680	0.000	0.002			G_PROTEIN_SIGNALING_COUPLED_TO_CYCLIC_NUCLEOTIDE_SECOND_MESSENGER	2.320	0.001	0.046
		POSITIVE_REGULATION_OF_I_KAPPAB_KINASE_NF_KAPPAB_CASCADE	2.570	0.000	0.005			RESPONSE_TO_WOUNDING	2.290	0.003	0.048
		PROTEIN_KINASE_CASCADE	2.570	0.000	0.004			CYCLIC_NUCLEOTIDE_MEDIATED_SIGNALING	2.220	0.004	0.067
		I_KAPPAB_KINASE_NF_KAPPAB_CASCADE	2.510	0.000	0.005			RESPONSE_TO_EXTERNAL_STIMULUS	2.200	0.000	0.068

		REGULATION_OF_I_KAPPAB_KINASE_NF_KAPPAB_CASCADE	2.470	0.000	0.007
		NEGATIVE_REGULATION_OF_DEVELOPMENTAL_PROCESS	2.450	0.000	0.007
		MEMBRANE_ORGANIZATION_AND_BIOGENESIS	2.420	0.001	0.009
		REGULATION_OF_APOPTOSIS	2.390	0.000	0.010
		REGULATION_OF_PROGRAMMED_CELL_DEATH	2.380	0.001	0.010
		APOPTOSIS_GO	2.350	0.000	0.012
		PROGRAMMED_CELL_DEATH	2.340	0.000	0.013
		VESICLE_MEDIATED_TRANSPORT	2.250	0.000	0.024
		POSITIVE_REGULATION_OF_SIGNAL_TRANSDUCTION	2.230	0.003	0.027
		REGULATION_OF_DEVELOPMENTAL_PROCESS	2.200	0.000	0.032
		HUMORAL_IMMUNE_RESPONSE	2.170	0.005	0.036
		POST_TRANSLATIONAL_PROTEIN_MODIFICATION	2.160	0.000	0.036
		MACROMOLECULE_CATABOLIC_PROCESS	2.110	0.004	0.048
	Knockout	TRANSLATION	-2.350	0.000	0.067
		CELLULAR_BIOSYNTHETIC_PROCESS	-2.030	0.000	0.251
		CENTRAL_NERVOUS_SYSTEM_DEVELOPMENT	-1.800	0.000	0.619
		DNA_REPLICATION	-1.730	0.022	0.658
		MITOCHONDRION_ORGANIZATION_AND_BIOGENESIS	-1.700	0.046	0.630
- Molecular function	Wild-Type	NUCLEOSIDE_TRIPHOSPHATASE_ACTIVITY	2.220	0.000	0.243
		GROWTH_FACTOR_ACTIVITY	2.130	0.003	0.206
		PROTEIN_BINDING_BRIDGING	2.090	0.002	0.184
		PYROPHOSPHATASE_ACTIVITY	2.080	0.005	0.147
		HYDROLASE_ACTIVITY_ACTING_ON_ACID_ANHYDRIDES	2.050	0.006	0.148
		TRANSMEMBRANE_RECEPTOR_ACTIVITY	2.040	0.002	0.131
		SH3_SH2_ADAPTOR_ACTIVITY	2.030	0.006	0.121
		TRANSCRIPTION_ACTIVATOR_ACTIVITY	2.030	0.006	0.108
		TRANSFERASE_ACTIVITY_TRANSFERRING_ACYL_GROUPS	2.020	0.000	0.100
		ION_CHANNEL_ACTIVITY	2.000	0.005	0.106
		GTPASE_BINDING	1.980	0.008	0.106
		ENZYME_BINDING	1.980	0.005	0.099
		GTPASE_ACTIVITY	1.960	0.009	0.098
		SUBSTRATE_SPECIFIC_CHANNEL_ACTIVITY	1.930	0.011	0.110
		ACTIN_BINDING	1.920	0.004	0.115
		GATED_CHANNEL_ACTIVITY	1.900	0.013	0.122
		G_PROTEIN_COUPLED_RECEPTOR_ACTIVITY	1.880	0.010	0.128
		SMALL_GTPASE_BINDING	1.880	0.008	0.121
		ENDOPEPTIDASE_ACTIVITY	1.860	0.016	0.132
		CATION_CHANNEL_ACTIVITY	1.850	0.015	0.127
	Knockout	STRUCTURAL_CONSTITUENT_OF_RIBOSOME	-4.650	0.000	0.000
		STRUCTURAL_MOLECULE_ACTIVITY	-3.240	0.000	0.000
		RNA_BINDING	-2.060	0.000	0.060
		NEUROTRANSMITTER_RECEPTOR_ACTIVITY	-1.810	0.015	0.215
		NEUROTRANSMITTER_BINDING	-1.740	0.018	0.263
- Cellular component	Wild-Type	EXTRACELLULAR_SPACE	2.630	0.000	0.005
		VESICLE	2.360	0.000	0.016
		MEMBRANE_BOUND_VESICLE	2.300	0.000	0.016
		GOLGI_ASSOCIATED_VESICLE	2.280	0.000	0.016
		CYTOPLASMIC_VESICLE	2.200	0.000	0.017
		CYTOPLASMIC_MEMBRANE_BOUND_VESICLE	2.190	0.001	0.016
		EXTRACELLULAR_REGION	2.190	0.001	0.013
		EXTRACELLULAR_REGION_PART	2.140	0.000	0.018
		ENDOSOME	2.100	0.001	0.020

		NEUROLOGICAL_SYSTEM_PROCESS	2.180	0.000	0.068
		LIPID_METABOLIC_PROCESS	2.160	0.001	0.068
		POST_TRANSLATIONAL_PROTEIN_MODIFICATION	2.130	0.001	0.078
		DEFENSE_RESPONSE	2.080	0.005	0.097
		G_PROTEIN_SIGNALING_COUPLED_TO_CAMP_NUCLEOTIDE_SECOND_MESSENGER	2.070	0.006	0.094
		CAMP_MEDIATED_SIGNALING	2.070	0.003	0.088
		REGULATION_OF_MAP_KINASE_ACTIVITY	2.070	0.006	0.085
		HUMORAL_IMMUNE_RESPONSE	2.050	0.005	0.092
		REGULATION_OF_MOLECULAR_FUNCTION	2.040	0.001	0.087
		MAPKKK_CASCADE_GO_0000165	2.040	0.001	0.082
		TRANSMISSION_OF_NERVE_IMPULSE	2.010	0.005	0.093
		POSITIVE_REGULATION_OF_IMMUNE_RESPONSE	2.010	0.000	0.093
		I_KAPPAB_KINASE_NF_KAPPAB_CASCADE	2.010	0.006	0.089
	Knockout	MICROTUBULE_CYTOSKELETON_ORGANIZATION_AND_BIOGENESIS	-2.380	0.000	0.074
		CELL_CYCLE_GO_0007049	-2.310	0.000	0.064
		GOLGI_VESICLE_TRANSPORT	-2.260	0.000	0.062
		CELL_CYCLE_PROCESS	-2.260	0.000	0.049
		DNA_METABOLIC_PROCESS	-2.220	0.000	0.046
		NEGATIVE_REGULATION_OF_TRANSCRIPTION_FROM_RNA_POLYMERASE_II_PROMOTER	-2.210	0.003	0.042
		RIBONUCLEOPROTEIN_COMPLEX_BIOGENESIS_AND_ASSEMBLY	-2.120	0.006	0.063
		PROTEIN_RNA_COMPLEX_ASSEMBLY	-2.060	0.003	0.076
		RNA_PROCESSING	-1.990	0.004	0.103
		MITOTIC_CELL_CYCLE	-1.990	0.000	0.094
		CELL_CYCLE_PHASE	-1.970	0.000	0.096
		ER_TO_GOLGI_VESICLE_MEDIATED_TRANSPORT	-1.970	0.007	0.088
		RNA_SPLICING	-1.950	0.003	0.093
		BIOPOLYMER_CATABOLIC_PROCESS	-1.920	0.004	0.103
		NERVOUS_SYSTEM_DEVELOPMENT	-1.890	0.007	0.110
		MACROMOLECULAR_COMPLEX_ASSEMBLY	-1.880	0.010	0.113
		INTERPHASE_OF_MITOTIC_CELL_CYCLE	-1.870	0.015	0.111
		POLYSACCHARIDE_METABOLIC_PROCESS	-1.850	0.014	0.116
		DNA_REPLICATION	-1.840	0.021	0.115
		PROTEIN_CATABOLIC_PROCESS	-1.840	0.018	0.110
- Molecular function	Wild-Type	G_PROTEIN_COUPLED_RECEPTOR_ACTIVITY	2.880	0.000	0.001
		RHODOPSIN_LIKE_RECEPTOR_ACTIVITY	2.490	0.000	0.013
		TRANSMEMBRANE_RECEPTOR_ACTIVITY	2.410	0.000	0.017
		METALLOENDOPEPTIDASE_ACTIVITY	2.140	0.003	0.085
		PEPTIDE_RECEPTOR_ACTIVITY	1.920	0.009	0.287
		PHOSPHOLIPID_BINDING	1.920	0.011	0.244
	Knockout	TRANSLATION_FACTOR_ACTIVITY_NUCLEIC_ACID_BINDING	-2.750	0.000	0.001
		TRANSLATION_REGULATOR_ACTIVITY	-2.620	0.000	0.003
		TRANSLATION_INITIATION_FACTOR_ACTIVITY	-2.390	0.000	0.012
		MICROTUBULE_MOTOR_ACTIVITY	-2.170	0.000	0.039
		MOTOR_ACTIVITY	-2.160	0.002	0.034
		NUCLEOTIDYLTRANSFERASE_ACTIVITY	-2.060	0.000	0.048
		SEQUENCE_SPECIFIC_DNA_BINDING	-2.000	0.012	0.060
		UNFOLDED_PROTEIN_BINDING	-1.840	0.012	0.142
		GUANYL_NUCLEOTIDE_EXCHANGE_FACTOR_ACTIVITY	-1.780	0.021	0.183
- Cellular component	Wild-Type	EXTRACELLULAR_SPACE	2.240	0.000	0.090
		EXTRACELLULAR_REGION_PART	2.150	0.000	0.077
		EXTRACELLULAR_REGION	2.110	0.001	0.066
		MITOCHONDRIAL_PART	2.060	0.001	0.073
		ENDOSOME	1.840	0.017	0.225
	Knockout	NUCLEAR_LUMEN	-1.850	0.014	0.699
		CYTOSKELETON	-1.800	0.000	0.494
		NUCLEOPLASM	-1.780	0.021	0.361

		LIPID_RAFT	1.840	0.016	0.096			ORGANELLE_LUMEN	-1.760	0.016	0.308
		NUCLEAR_MEMBRANE	1.800	0.019	0.109			GOLGI_APPARATUS	-1.750	0.010	0.259
		GOLGI_APPARATUS	1.800	0.014	0.103						
		VACUOLE	1.740	0.019	0.126						
		LYTIC_VACUOLE	1.740	0.024	0.121						
		LYSOSOME	1.720	0.030	0.122						
		CYTOPLASMIC_VESICLE_MEMBRANE	1.720	0.028	0.118						
		CELL_FRACTION	1.700	0.019	0.122						
		CYTOPLASMIC_VESICLE_PART	1.690	0.024	0.123						
		COATED_VESICLE	1.680	0.031	0.119						
		PEROXISOME	1.680	0.030	0.115						
	Knockout	ORGANELLAR_RIBOSOME	-3.490	0.000	0.000						
		MITOCHONDRIAL_RIBOSOME	-3.370	0.000	0.000						
		RIBOSOMAL_SUBUNIT	-3.020	0.000	0.000						
		RIBOSOME	-2.940	0.000	0.000						
		MITOCHONDRIAL_PART	-2.910	0.000	0.000						
		MITOCHONDRION	-2.880	0.000	0.000						
		RIBONUCLEOPROTEIN_COMPLEX	-2.770	0.000	0.000						
		MITOCHONDRIAL_MEMBRANE_PART	-2.770	0.000	0.000						
		MITOCHONDRIAL_LUMEN	-2.540	0.000	0.002						
		MITOCHONDRIAL_RESPIRATORY_CHAIN	-2.490	0.000	0.002						
		MITOCHONDRIAL_MATRIX	-2.420	0.000	0.002						
		RESPIRATORY_CHAIN_COMPLEX_I	-2.310	0.000	0.004						
		NADH_DEHYDROGENASE_COMPLEX	-2.310	0.000	0.004						
		MITOCHONDRIAL_RESPIRATORY_CHAIN_COMPLEX_I	-2.300	0.000	0.004						
		MITOCHONDRIAL_INNER_MEMBRANE	-2.140	0.003	0.010						
		CHROMOSOME	-2.110	0.000	0.012						
		ORGANELLE_LUMEN	-2.080	0.009	0.013						
		ORGANELLE_INNER_MEMBRANE	-2.080	0.000	0.012						
		SMALL_NUCLEAR_RIBONUCLEOPROTEIN_COMPLEX	-2.050	0.010	0.014						
		MEMBRANE_ENCLOSED_LUMEN	-2.030	0.000	0.014						
Oncogenic pathway targets	Wild-Type	RPS14_DN.V1_UP	3.750	0.000	0.000	Oncogenic pathway targets	Wild-Type	RPS14_DN.V1_UP	3.570	0.000	0.000
		HOXA9_DN.V1_UP	3.500	0.000	0.000			HINATA_NFKB_IMMU_INF	3.000	0.000	0.000
		EGFR_UP.V1_UP	3.460	0.000	0.000			SNF5_DN.V1_UP	2.950	0.000	0.000
		STK33_NOMO_UP	3.210	0.000	0.000			E2F1_UP.V1_DN	2.910	0.000	0.000
		STK33_UP	3.050	0.000	0.000			STK33_SKM_UP	2.820	0.000	0.000
		E2F1_UP.V1_DN	2.990	0.000	0.000			MTOR_UP.N4.V1_UP	2.800	0.000	0.000
		STK33_SKM_UP	2.890	0.000	0.000			CSR_LATE_UP.V1_DN	2.750	0.000	0.000
		CSR_EARLY_UP.V1_UP	2.740	0.000	0.000			STK33_NOMO_UP	2.390	0.001	0.007
		CSR_LATE_UP.V1_DN	2.680	0.000	0.000			STK33_UP	2.360	0.001	0.007
		TBK1.DF_DN	2.620	0.001	0.001			PRC2_EZH2_UP.V1_DN	2.340	0.000	0.007
		TBK1.DN.48HRS_DN	2.580	0.000	0.001			EGFR_UP.V1_UP	2.260	0.000	0.012
		BMI1_DN_MEL18_DN.V1_DN	2.480	0.000	0.003			MEL18_DN.V1_UP	2.220	0.001	0.014
		CORDENONSI_YAP_CONSERVED_SIGNATURE	2.470	0.000	0.002			KRAS.600.LUNG.BREAST_UP.V1_UP	2.160	0.000	0.019
		ESC_J1_UP_LATE.V1_UP	2.400	0.001	0.003			HOXA9_DN.V1_UP	2.040	0.005	0.039
		PRC2_EZH2_UP.V1_DN	2.330	0.000	0.005			BCAT_BILD_ET_AL_UP	2.000	0.002	0.046
		RB_P107_DN.V1_DN	2.300	0.001	0.006			CAHOY_NEURONAL	1.990	0.006	0.048
		AKT_UP_MTOR_DN.V1_UP	2.240	0.000	0.009			ERB2_UP.V1_UP	1.940	0.009	0.063
		HINATA_NFKB_IMMU_INF	2.210	0.000	0.010			BMI1_DN_MEL18_DN.V1_DN	1.930	0.008	0.061
		AKT_UP.V1_UP	2.200	0.003	0.010			LTE2_UP.V1_UP	1.900	0.005	0.070
		RB_P130_DN.V1_DN	2.170	0.003	0.011			MTOR_UP.V1_UP	1.900	0.012	0.067
	Knockout	RB_P107_DN.V1_UP	-4.800	0.000	0.000		Knockout	RB_P107_DN.V1_UP	-3.510	0.000	0.000
		ATF2_UP.V1_UP	-2.210	0.005	0.016			CAMP_UP.V1_UP	-2.480	0.000	0.002
		RB_DN.V1_UP	-2.180	0.000	0.013			CSR_LATE_UP.V1_UP	-2.390	0.000	0.003
		PRC2_EDD_UP.V1_UP	-1.930	0.005	0.046			ESC_V6.5_UP_LATE.V1_DN	-2.090	0.004	0.020
		CSR_EARLY_UP.V1_DN	-1.920	0.000	0.038			RPS14_DN.V1_DN	-1.920	0.000	0.045
		RB_P130_DN.V1_UP	-1.790	0.011	0.067			RB_P130_DN.V1_UP	-1.630	0.035	0.172
		EIF4E_UP	-1.550	0.054	0.201			PRC2_EDD_UP.V1_UP	-1.630	0.032	0.150
		BRCA1_DN.V1_UP	-1.510	0.083	0.219			ESC_V6.5_UP_EARLY.V1_DN	-1.530	0.068	0.215
		KRAS.AMP.LUNG_UP.V1_UP	-1.500	0.053	0.202			AKT_UP.V1_DN	-1.500	0.041	0.219
		RPS14_DN.V1_DN	-1.430	0.076	0.246			SNF5_DN.V1_DN	-1.500	0.059	0.203
								TGFB_UP.V1_UP	-1.470	0.075	0.210
								E2F1_UP.V1_UP	-1.440	0.086	0.217
								RB_DN.V1_UP	-1.420	0.081	0.220
								EIF4E_DN	-1.390	0.104	0.224
Immunologic pathway targets	Wild-Type	GSE22886_NAIVE_TCELL_VS_MONOCYTE_DN	5.600	0.000	0.000	Immunologic pathway targets	Wild-Type	GSE24634_TREG_VS_TCONV_POST_DAY3_IL4_CONVERSION_DN	4.700	0.000	0.000
		GSE22886_NAIVE_BCELL_VS_MONOCYTE_DN	5.510	0.000	0.000			GSE29618_MONOCYTE_VS_PDC_UP	4.490	0.000	0.000
		GSE29618_MONOCYTE_VS_PDC_UP	5.400	0.000	0.000			GSE29618_PDC_VS_MDC_DN	4.470	0.000	0.000
		GSE22886_NAIVE_CD4_TCELL_VS_MONOCYTE_DN	5.350	0.000	0.000			GSE22886_NAIVE_CD4_TCELL_VS_MONOCYTE_DN	4.460	0.000	0.000
		GSE22886_NAIVE_CD8_TCELL_VS_MONOCYTE_DN	5.290	0.000	0.000			GSE10325_LUPUS_CD4_TCELL_VS_LUPUS_MYELOID_DN	4.440	0.000	0.000
		GSE10325_LUPUS_CD4_TCELL_VS_LUPUS_MYELOID_DN	5.210	0.000	0.000			GSE10325_LUPUS_BCELL_VS_LUPUS_MYELOID_DN	4.240	0.000	0.000
		GSE29618_PDC_VS_MDC_DN	5.200	0.000	0.000			GSE29618_MONOCYTE_VS_MDC_UP	4.210	0.000	0.000

		GSE29618_PDC_VS_MDC_DAY7_FLU_VACCINE_DN	5.010	0.000	0.000			GSE22886_NAIVE_BCELL_VS_MONOCYTE_DN	4.180	0.000	0.000
		GSE29618_MONOCYTE_VS_MDC_DAY7_FLU_VACCINE_UP	4.980	0.000	0.000			GSE29618_PDC_VS_MDC_DAY7_FLU_VACCINE_DN	4.140	0.000	0.000
		GSE24634_TREG_VS_TCONV_POST_DAY3_IL4_CONVERSION_DN	4.790	0.000	0.000			GSE29618_MONOCYTE_VS_PDC_DAY7_FLU_VACCINE_UP	4.070	0.000	0.000
		GSE29618_MONOCYTE_VS_MDC_UP	4.780	0.000	0.000			GSE10325_BCELL_VS_MYELOID_DN	3.910	0.000	0.000
		GSE22886_NAIVE_TCELL_VS_DC_DN	4.760	0.000	0.000			GSE24634_TREG_VS_TCONV_POST_DAY10_IL4_CONVERSION_DN	3.880	0.000	0.000
		GSE10325_BCELL_VS_MYELOID_DN	4.650	0.000	0.000			GSE24142_EARLY_THYMIC_PROGENITOR_VS_DN2_THYMOCYTE_ADULT_UP	3.850	0.000	0.000
		GSE29618_MONOCYTE_VS_PDC_DAY7_FLU_VACCINE_UP	4.640	0.000	0.000			GSE22886_NAIVE_CD8_TCELL_VS_MONOCYTE_DN	3.850	0.000	0.000
		GSE22886_NAIVE_CD8_TCELL_VS_DC_DN	4.580	0.000	0.000			GSE22886_NAIVE_TCELL_VS_MONOCYTE_DN	3.840	0.000	0.000
		GSE10325_LUPUS_BCELL_VS_LUPUS_MYELOID_DN	4.520	0.000	0.000			GSE6269_HEALTHY_VS_STREP_AUREUS_INF_PBMC_DN	3.820	0.000	0.000
		GSE24634_TEFF_VS_TCONV_DAY7_IN_CULTURE_DN	4.460	0.000	0.000			GSE29618_MONOCYTE_VS_MDC_DAY7_FLU_VACCINE_UP	3.790	0.000	0.000
		GSE29618_BCELL_VS_MONOCYTE_DAY7_FLU_VACCINE_DN	4.440	0.000	0.000			GSE24142_EARLY_THYMIC_PROGENITOR_VS_DN2_THYMOCYTE_UP	3.730	0.000	0.000
		GSE10325_CD4_TCELL_VS_MYELOID_DN	4.280	0.000	0.000			GSE29618_BCELL_VS_MONOCYTE_DAY7_FLU_VACCINE_DN	3.650	0.000	0.000
		GSE22886_NAIVE_BCELL_VS_DC_DN	4.260	0.000	0.000			GSE9988_ANTI_TREM1_VS_LPS_MONOCYTE_DN	3.640	0.000	0.000
	Knockout	KAECH_DAY8_EFF_VS_DAY15_EFF_CD8_TCELL_UP	-4.070	0.000	0.000		Knockout	GSE15930_NAIVE_VS_48H_IN_VITRO_STIM_CD8_TCELL_DN	-3.480	0.000	0.000
		GSE15750_DAY6_VS_DAY10_TRAF6KO_EFF_CD8_TCELL_UP	-3.940	0.000	0.000			GSE36476_CTRL_VS_TSST_ACT_40H_MEMORY_CD4_TCELL_OLD_DN	-3.440	0.000	0.000
		GSE39820_TGFBETA1_IL6_VS_TGFBETA1_IL6_IL23A_TREATED_CD4_TCELL_DN	-3.850	0.000	0.000			GSE15750_DAY6_VS_DAY10_TRAF6KO_EFF_CD8_TCELL_UP	-3.350	0.000	0.000
		GSE15750_DAY6_VS_DAY10_EFF_CD8_TCELL_UP	-3.830	0.000	0.000			GSE9650_NAIVE_VS_EXHAUSTED_CD8_TCELL_UP	-3.340	0.000	0.000
		GSE17974_CTRL_VS_ACT_IL4_AND_ANTI_IL12_48H_CD4_TCELL_DN	-3.610	0.000	0.000			GSE1460_DP_THYMOCYTE_VS_NAIVE_CD4_TCELL_CORD_BLOOD_UP	-3.120	0.000	0.000
		GSE9650_EFFECTOR_VS_MEMORY_CD8_TCELL_UP	-3.510	0.000	0.000			GSE15750_DAY6_VS_DAY10_EFF_CD8_TCELL_UP	-3.050	0.000	0.000
		GSE19825_NAIVE_VS_DAY3_EFF_CD8_TCELL_DN	-3.390	0.000	0.000			GSE24634_TEFF_VS_TCONV_DAY3_IN_CULTURE_UP	-2.890	0.000	0.000
		GSE15930_NAIVE_VS_48H_IN_VITRO_STIM_CD8_TCELL_DN	-3.340	0.000	0.000			GSE17974_CTRL_VS_ACT_IL4_AND_ANTI_IL12_48H_CD4_TCELL_DN	-2.830	0.000	0.000
		GSE15930_NAIVE_VS_72H_IN_VITRO_STIM_TRICHOSTATINA_CD8_TCELL_DN	-3.250	0.000	0.000			GSE24634_TEFF_VS_TCONV_DAY5_IN_CULTURE_UP	-2.800	0.000	0.001
		GSE24634_TREG_VS_TCONV_POST_DAY7_IL4_CONVERSION_UP	-3.200	0.000	0.000			GSE36476_CTRL_VS_TSST_ACT_72H_MEMORY_CD4_TCELL_OLD_DN	-2.770	0.000	0.001
		GSE17721_0.5H_VS_12H_LPS_BMDM_UP	-3.160	0.000	0.000			GSE3337_4H_VS_16H_IFNG_IN_CD8POS_DC_UP	-2.700	0.000	0.001
		GSE9006_TYPE_1_DIABETES_AT_DX_VS_4MONTH_POST_DX_PBMC_DN	-3.070	0.000	0.000			GSE10239_KLRG1INT_VS_KLRG1HIGH_EFF_CD8_TCELL_UP	-2.670	0.000	0.001
		GSE36476_CTRL_VS_TSST_ACT_40H_MEMORY_CD4_TCELL_OLD_DN	-3.050	0.000	0.000			GSE1460_INTRATHYMIC_T_PROGENITOR_VS_NAIVE_CD4_TCELL_ADULT_BLOOD_UP	-2.650	0.000	0.001
		GSE24634_TEFF_VS_TCONV_DAY5_IN_CULTURE_UP	-3.040	0.000	0.000			GSE10239_NAIVE_VS_KLRG1HIGH_EFF_CD8_TCELL_DN	-2.650	0.000	0.001
		GSE30962_PRIMARY_VS_SECONDARY_ACUTE_LCMV_INF_CD8_TCELL_UP	-3.030	0.000	0.000			GSE36476_CTRL_VS_TSST_ACT_40H_MEMORY_CD4_TCELL_YOUNG_DN	-2.630	0.000	0.001
		GSE15930_STIM_VS_STIM_AND_IFNAB_48H_CD8_T_CELL_UP	-2.970	0.000	0.000			GSE30962_PRIMARY_VS_SECONDARY_ACUTE_LCMV_INF_CD8_TCELL_UP	-2.600	0.000	0.002
		GSE36476_CTRL_VS_TSST_ACT_72H_MEMORY_CD4_TCELL_YOUNG_DN	-2.940	0.000	0.000			GSE17721_CPG_VS_GARDIQUIMOD_1H_BMDM_DN	-2.540	0.000	0.002
		GSE31082_DN_VS_DP_THYMOCYTE_UP	-2.910	0.000	0.000			GSE9650_GP33_VS_GP276_LCMV_SPECIFIC_EXHAUSTED_CD8_TCELL_DN	-2.500	0.000	0.003
		GSE14000_TRANSLATED_RNA_VS_MRNA_16H_LPS_DC_DN	-2.910	0.000	0.000			GSE12366_PLASMA_CELL_VS_MEMORY_BCELL_UP	-2.490	0.000	0.003
		GSE17721_PAM3CSK4_VS_CPG_12H_BMDM_UP	-2.870	0.000	0.000			GSE20715_0H_VS_48H_OZONE_LUNG_DN	-2.490	0.000	0.003
Genes co-expressed with cancer-related genes	Wild-Type	GNF2_HCK	4.540	0.000	0.000	Genes co-expressed with cancer-related genes	Wild-Type	GNF2_HCK	4.490	0.000	0.000
		GNF2_CASP1	4.510	0.000	0.000			GNF2_TNFRSF1B	4.350	0.000	0.000
		GNF2_TNFRSF1B	4.450	0.000	0.000			GNF2_CASP1	4.280	0.000	0.000
		GNF2_CARD15	4.340	0.000	0.000			GNF2_PECAM1	3.750	0.000	0.000
		GNF2_MYD88	4.030	0.000	0.000			GNF2_ITGB2	3.680	0.000	0.000
		GNF2_SELL	4.000	0.000	0.000			GNF2_CARD15	3.630	0.000	0.000
		GNF2_PECAM1	3.910	0.000	0.000			GNF2_STAT6	3.530	0.000	0.000
		GNF2_SPI1	3.810	0.000	0.000			GNF2_SELL	3.520	0.000	0.000
		GNF2_STAT6	3.810	0.000	0.000			GNF2_MCL1	3.390	0.000	0.000
		GNF2_PTPRC	3.710	0.000	0.000			GNF2_TNFSF10	3.380	0.000	0.000
		MORF_PAPSS1	3.620	0.000	0.000			GNF2_CD1D	3.360	0.000	0.000
		GNF2_CD33	3.540	0.000	0.000			GNF2_MYD88	3.300	0.000	0.000
		GNF2_MCL1	3.510	0.000	0.000			GNF2_CD33	3.220	0.000	0.000
		GNF2_ITGB2	3.490	0.000	0.000			GNF2_S100A4	3.150	0.000	0.000
		GNF2_CD1D	3.400	0.000	0.000			GNF2_FGR	3.150	0.000	0.000
		GNF2_S100A4	3.370	0.000	0.000			GNF2_CD53	3.070	0.000	0.000
		GNF2_TYK2	3.310	0.000	0.000			GNF2_SPI1	3.010	0.000	0.000
		GNF2_CD14	3.290	0.000	0.000			GNF2_CD97	3.000	0.000	0.000
		GNF2_TNFSF10	3.250	0.000	0.000			GNF2_CD14	2.940	0.000	0.000
		MORF_SP3	3.200	0.000	0.000			GNF2_PTPRC	2.720	0.000	0.000
	Knockout	MORF_NME2	-4.150	0.000	0.000		Knockout	MORF_CSNK2B	-3.030	0.000	0.000

		GNF2_EIF3S6	-3.930	0.000	0.000			MORF_BUB3	-3.020	0.000	0.000
		GNF2_GLTSCR2	-3.570	0.000	0.000			MORF_SOD1	-2.750	0.000	0.002
		GCM_TPT1	-3.440	0.000	0.000			MORF_RAD23A	-2.700	0.000	0.002
		MORF_TPT1	-3.280	0.000	0.000			GNF2_RRM1	-2.690	0.000	0.002
		MORF_NPM1	-3.170	0.000	0.000			GNF2_CENPF	-2.690	0.000	0.002
		GCM_NPM1	-3.130	0.000	0.000			GNF2_RRM2	-2.600	0.000	0.003
		MORF_JUND	-3.080	0.000	0.000			GNF2_MCM4	-2.590	0.000	0.003
		GNF2_MCM4	-3.060	0.000	0.000			GNF2_RFC3	-2.570	0.000	0.004
		MORF_ACTG1	-3.030	0.000	0.000			MORF_FEN1	-2.560	0.000	0.004
		MORF_RAN	-3.000	0.000	0.000			MORF_CCNF	-2.500	0.000	0.004
		MORF_ANP32B	-2.960	0.000	0.000			MORF_PPP5C	-2.490	0.003	0.004
		MORF_PSMC1	-2.820	0.000	0.000			GNF2_CENPE	-2.480	0.000	0.005
		GNF2_CENPF	-2.790	0.000	0.000			GCM_GSPT1	-2.470	0.000	0.004
		MORF_CSNK2B	-2.770	0.000	0.000			MORF_RAD54L	-2.470	0.000	0.004
		MORF_PPP1CA	-2.760	0.000	0.000			MORF_RAC1	-2.390	0.000	0.006
		GNF2_CCNA2	-2.760	0.000	0.000			MORF_PSMC1	-2.370	0.000	0.008
		GNF2_DAP3	-2.750	0.000	0.000			MORF_PPP1CA	-2.350	0.004	0.008
		GNF2_PCNA	-2.710	0.000	0.000			MORF_MTA1	-2.330	0.000	0.008
		GNF2_RRM2	-2.660	0.000	0.000			GCM_BMPR2	-2.330	0.003	0.008
Chemical and genetic perturbations	Wild-Type	FULCHER_INFLAMMATORY_RESPONSE_LECTIN_VS_LPS_DN	5.040	0.000	0.000	Chemical and genetic perturbations	Wild-Type	ICHIBA_GRAFT_VERSUS_HOST_DISEASE_35D_UP	4.730	0.000	0.000
(Experimentally defined target gene signature		MCLACHLAN_DENTAL_CARIES_UP	5.040	0.000	0.000	(Experimentally defined target gene signature		HOSHIDA_LIVER_CANCER_SUBCLASS_S1	4.650	0.000	0.000
in literature)		OSMAN_BLADDER_CANCER_UP	4.750	0.000	0.000	in literature)		HESS_TARGETS_OF_HOXA9_AND_MEIS1_DN	4.650	0.000	0.000
		HOSHIDA_LIVER_CANCER_SUBCLASS_S1	4.700	0.000	0.000			MARKEY_RB1_ACUTE_LOF_UP	4.630	0.000	0.000
		THUM_SYSTOLIC_HEART_FAILURE_UP	4.600	0.000	0.000			MCLACHLAN_DENTAL_CARIES_UP	4.550	0.000	0.000
		HESS_TARGETS_OF_HOXA9_AND_MEIS1_DN	4.580	0.000	0.000			RODWELL_AGING_KIDNEY_UP	4.440	0.000	0.000
		MORI_MATURE_B_LYMPHOCYTE_UP	4.520	0.000	0.000			LINDGREN_BLADDER_CANCER_CLUSTER_2B	4.250	0.000	0.000
		MCLACHLAN_DENTAL_CARIES_DN	4.520	0.000	0.000			SCHUETZ_BREAST_CANCER_DUCTAL_INVASIVE_UP	4.230	0.000	0.000
		VERHAAK_GLIOBLASTOMA_NEURAL	4.500	0.000	0.000			QI_PLASMACYTOMA_UP	4.210	0.000	0.000
		ICHIBA_GRAFT_VERSUS_HOST_DISEASE_35D_UP	4.430	0.000	0.000			VERHAAK_GLIOBLASTOMA_NEURAL	4.180	0.000	0.000
		MARKEY_RB1_ACUTE_LOF_UP	4.420	0.000	0.000			IGLESIAS_E2F_TARGETS_UP	4.110	0.000	0.000
		SCHUETZ_BREAST_CANCER_DUCTAL_INVASIVE_UP	4.410	0.000	0.000			PICCALUGA_ANGIOIMMUNOBLASTIC_LYMPHOMA_UP	4.100	0.000	0.000
		MILI_PSEUDOPODIA_CHEMOTAXIS_DN	4.350	0.000	0.000			MCLACHLAN_DENTAL_CARIES_DN	4.040	0.000	0.000
		LINDGREN_BLADDER_CANCER_CLUSTER_2B	4.320	0.000	0.000			SWEET_LUNG_CANCER_KRAS_UP	4.020	0.000	0.000
		IGLESIAS_E2F_TARGETS_UP	4.290	0.000	0.000			FULCHER_INFLAMMATORY_RESPONSE_LECTIN_VS_LPS_DN	3.980	0.000	0.000
		FLECHNER_BIOPSY_KIDNEY_TRANSPLANT_OK_VS_DONOR_UP	4.240	0.000	0.000			ICHIBA_GRAFT_VERSUS_HOST_DISEASE_D7_UP	3.950	0.000	0.000
		REN_ALVEOLAR_RHABDOMYOSARCOMA_DN	4.240	0.000	0.000			HORTON_SREBF_TARGETS	3.930	0.000	0.000
		RUTELLA_RESPONSE_TO_HGF_VS_CSF2RB_AND_IL4_UP	4.230	0.000	0.000			SCHMIDT_POR_TARGETS_IN_LIMB_BUD_UP	3.900	0.000	0.000
		QI_PLASMACYTOMA_UP	4.220	0.000	0.000			VERHAAK_AML_WITH_NPM1_MUTATED_UP	3.840	0.000	0.000
		PASINI_SUZ12_TARGETS_DN	4.110	0.000	0.000			ALTEMEIER_RESPONSE_TO_LPS_WITH_MECHANICAL_VENTILATION	3.830	0.000	0.000
	Knockout	GOBERT_OLIGODENDROCYTE_DIFFERENTIATION_UP	-5.680	0.000	0.000		Knockout	GOBERT_OLIGODENDROCYTE_DIFFERENTIATION_UP	-5.140	0.000	0.000
		STARK_PREFRONTAL_CORTEX_22Q11_DELETION_DN	-4.800	0.000	0.000			MARKEY_RB1_ACUTE_LOF_DN	-4.480	0.000	0.000
		CUI_TCF21_TARGETS_2_UP	-4.530	0.000	0.000			BERENJENO_TRANSFORMED_BY_RHOA_UP	-4.290	0.000	0.000
		YAO_TEMPORAL_RESPONSE_TO_PROGESTERONE_CLUSTER_13	-4.470	0.000	0.000			BASAKI_YBX1_TARGETS_UP	-3.920	0.000	0.000
		LU_EZH2_TARGETS_UP	-4.370	0.000	0.000			WONG_EMBRYONIC_STEM_CELL_CORE	-3.780	0.000	0.000
		WONG_EMBRYONIC_STEM_CELL_CORE	-4.260	0.000	0.000			BLUM_RESPONSE_TO_SALIRASIB_DN	-3.410	0.000	0.000
		MOOTHA_VOXPHOS	-4.190	0.000	0.000			BURTON_ADIPOGENESIS_3	-3.370	0.000	0.000
		DUTERTRE_ESTRADIOL_RESPONSE_24HR_UP	-3.920	0.000	0.000			YAO_TEMPORAL_RESPONSE_TO_PROGESTERONE_CLUSTER_14	-3.290	0.000	0.000
		DAIRKEE_TERT_TARGETS_UP	-3.770	0.000	0.000			DUTERTRE_ESTRADIOL_RESPONSE_24HR_UP	-3.200	0.000	0.000
		MOOTHA_HUMAN_MITODB_6_2002	-3.760	0.000	0.000			CROONQUIST_NRAS_SIGNALING_DN	-3.150	0.000	0.000
		YAO_TEMPORAL_RESPONSE_TO_PROGESTERONE_CLUSTER_17	-3.690	0.000	0.000			FOURNIER_ACINAR_DEVELOPMENT_LATE_2	-3.130	0.000	0.000
		BASAKI_YBX1_TARGETS_UP	-3.670	0.000	0.000			KOBAYASHI_EGFR_SIGNALING_24HR_DN	-3.110	0.000	0.000
		ROSTY_CERVICAL_CANCER_PROLIFERATION_CLUSTER	-3.660	0.000	0.000			WHITEFORD_PEDIATRIC_CANCER_MARKERS	-3.100	0.000	0.000
		CHICAS_RB1_TARGETS_LOW_SERUM	-3.610	0.000	0.000			HOFFMANN_LARGE_TO_SMALL_PRE_BII_LYMPHOCYTE_UP	-3.030	0.000	0.000
		LI_DCP2_BOUND_MRNA	-3.560	0.000	0.000			ISHIDA_E2F_TARGETS	-3.020	0.000	0.000
		ENK_UV_RESPONSE_KERATINOCYTE_UP	-3.550	0.000	0.000			RHODES_UNDIFFERENTIATED_CANCER	-2.990	0.000	0.000
		BERENJENO_TRANSFORMED_BY_RHOA_DN	-3.460	0.000	0.000			MISSIAGLIA_REGULATED_BY_METHYLATION_DN	-2.950	0.000	0.000
		WONG_MITOCHONDRIA_GENE_MODULE	-3.420	0.000	0.000			SOTIRIOU_BREAST_CANCER_GRADE_1_VS_3_UP	-2.940	0.000	0.000
		BLUM_RESPONSE_TO_SALIRASIB_DN	-3.420	0.000	0.000			MORI_LARGE_PRE_BII_LYMPHOCYTE_UP	-2.910	0.000	0.000
		MOOTHA_MITOCHONDRIA	-3.410	0.000	0.000			SHEDDEN_LUNG_CANCER_POOR_SURVIVAL_A6	-2.910	0.000	0.000
Transcription factor targets	Wild-Type	V$SRF_Q5_01	2.530	0.000	0.027	Transcription factor targets	Wild-Type	V$SRF_C	2.710	0.000	0.008
		V$CEBP_Q2_01	2.480	0.000	0.026			V$SRF_Q5_01	2.510	0.000	0.020
		V$ELF1_Q6	2.440	0.000	0.023			GGGNNTTTCC_V$NFKB_Q6_01	2.490	0.000	0.016
		V$USF_01	2.390	0.000	0.030			V$NFKAPPAB_01	2.350	0.000	0.041
		V$SRF_C	2.350	0.000	0.034			RGTTAMWNATT_V$HNF1_01	2.340	0.000	0.036
		CGGAARNGGCNG_UNKNOWN	2.340	0.001	0.033			V$SRF_Q4	2.300	0.003	0.040
		V$CEBPB_02	2.330	0.000	0.028			V$SRF_Q6	2.240	0.000	0.053
		V$SRF_01	2.320	0.000	0.027			V$SRF_01	2.230	0.002	0.050

		V$NFKAPPAB_01	2.290	0.000	0.030			V$STAT6_02	2.220	0.000	0.047
		V$SRF_Q4	2.280	0.003	0.028			V$CREL_01	2.210	0.000	0.046
		V$IRF_Q6	2.280	0.002	0.027			RGAGGAARY_V$PU1_Q6	2.190	0.002	0.049
		RGAGGAARY_V$PU1_Q6	2.270	0.000	0.027			V$NFKB_Q6	2.170	0.000	0.054
		V$CEBP_Q2	2.210	0.000	0.038			V$HNF1_01	2.160	0.000	0.052
		V$PEA3_Q6	2.190	0.001	0.040			RTTTNNNYTGGM_UNKNOWN	2.150	0.001	0.055
		V$FREAC7_01	2.190	0.003	0.039			$MTTTTTGT_UNKNOWN	2.120	0.000	0.065
		CGTSACG_V$PAX3_B	2.180	0.004	0.039			CTGRYYYNATT_UNKNOWN	2.090	0.001	0.071
		GCCATNTTG_V$YY1_Q6	2.170	0.000	0.040			STTTCRNTTT_V$IRF_Q6	2.090	0.001	0.069
		V$PAX4_04	2.170	0.000	0.038			V$USF_Q6	2.080	0.000	0.072
		V$FOXD3_01	2.160	0.005	0.040			V$NFKB_Q6_01	2.050	0.004	0.080
		V$NFMUE1_Q6	2.160	0.004	0.038			V$ELF1_Q6	2.040	0.005	0.084
	Knockout	KRCTCNNNNMANAGC_UNKNOWN	-2.800	0.000	0.000		Knockout	GGGNRMNNYCAT_UNKNOWN	-2.550	0.000	0.010
		RACTNNRTTTNC_UNKNOWN	-2.120	0.000	0.064			V$HSF_Q6	-2.500	0.000	0.008
		SGCGSSAAA_V$E2F1DP2_01	-1.910	0.004	0.154			RRCCGTTA_UNKNOWN	-2.080	0.000	0.103
		GGAANCGGAANY_UNKNOWN	-1.880	0.010	0.139			TTCNRGNNNNTTC_V$HSF_Q6	-1.980	0.000	0.141
		V$CP2_01	-1.740	0.012	0.233			V$SF1_Q6	-1.890	0.016	0.187
		GGAMTNNNNNTCCY_UNKNOWN	-1.720	0.008	0.220			V$SREBP1_01	-1.760	0.015	0.323
		GGGNRMNNYCAT_UNKNOWN	-1.720	0.023	0.190						
microRNA targets	Wild-Type	TTGCCAA,MIR-182	3.590	0.000	0.000	microRNA targets	Wild-Type	TAGCTTT,MIR-9	2.550	0.000	0.011
		CAGTATT,MIR-200B,MIR-200C,MIR-429	3.120	0.000	0.000			GTCAGGA,MIR-378	2.080	0.002	0.204
		TTTGCAC,MIR-19A,MIR-19B	2.990	0.000	0.000			TGCCTTA,MIR-124A	2.050	0.001	0.173
		TAATGTG,MIR-323	2.970	0.000	0.000			ATGTAGC,MIR-221,MIR-222	2.030	0.003	0.160
		GTGACTT,MIR-224	2.910	0.000	0.000			TTGGAGA,MIR-515-5P,MIR-519E	2.010	0.003	0.144
		TAGCTTT,MIR-9	2.840	0.000	0.000			TTGGGAG,MIR-150	2.000	0.011	0.124
		ACTGTAG,MIR-139	2.790	0.000	0.001			TTTGCAC,MIR-19A,MIR-19B	1.940	0.004	0.155
		GCAAAAA,MIR-129	2.780	0.000	0.000			ACATTCC,MIR-1,MIR-206	1.860	0.007	0.219
		TTGGAGA,MIR-515-5P,MIR-519E	2.780	0.000	0.000						
		TGCCTTA,MIR-124A	2.770	0.000	0.000		Knockout	GAGACTG,MIR-452	-2.220	0.007	0.045
		ACCATTT,MIR-522	2.710	0.000	0.000			ACACTGG,MIR-199A,MIR-199B	-1.580	0.046	0.756
		ATACTGT,MIR-144	2.650	0.000	0.000			GCTCTTG,MIR-335	-1.580	0.037	0.511
		TGCTTTG,MIR-330	2.540	0.000	0.001			AGTCAGC,MIR-345	-1.460	0.083	0.679
		GTTATAT,MIR-410	2.540	0.000	0.001			TCTAGAG,MIR-517	-1.430	0.088	0.612
		ACATTCC,MIR-1,MIR-206	2.530	0.000	0.001						
		AATGTGA,MIR-23A,MIR-23B	2.520	0.001	0.001						
		AAGCCAT,MIR-135A,MIR-135B	2.510	0.000	0.001						
		TTGCACT,MIR-130A,MIR-301,MIR-130B	2.480	0.001	0.001						
		TGAATGT,MIR-181A,MIR-181B,MIR-181C,MIR-181D	2.480	0.000	0.001						
		ACTGAAA,MIR-30A-3P,MIR-30E-3P	2.470	0.000	0.001						
	Knockout	CGCTGCT,MIR-503	-0.240	-1.300	0.169						
		CCTGAGT,MIR-510	-0.150	-1.130	0.276						
		GCAAGAC,MIR-431	-0.140	-1.010	0.422						
		GTGTCAA,MIR-514	-0.100	-0.900	0.534						
		AGCTCCT,MIR-28	-0.070	-0.810	0.702						

Supplementary table 4

Ingenuity pathway analysis for overexpressed genes in Pdgfrb-wild type hepatic stellate cells compared to knockout without Pdgfb treatment.

Analysis Name: ntpsig_noPdgfb_WT_vs_KO_cv0.1_cmsTp100_direction_corrected - 2013-11-15 07:31 AM
Analysis Creation Date: 2013-11-15
Build version: 242990
Content version: 17199142 (Release Date: 2013-09-17)

Analysis settings

View

Reference set: Ingenuity Knowledge Base (Genes Only)
Relationship to include: Direct and Indirect
Includes Endogenous Chemicals
Optional Analyses: My Pathways My List

Filter Summary:
Consider only relationships where
confidence = Experimentally Observed
Cutoff:

Top Networks

ID	Associated Network Functions	Score
1	Cell-To-Cell Signaling and Interaction, Hematological System Development and Function, Immune Cell Trafficking	38
2	Hematological Disease, Immunological Disease, Infectious Disease	38
3	Dermatological Diseases and Conditions, Hereditary Disorder, Organismal Injury and Abnormalities	31
4	Auditory Disease, Cellular Assembly and Organization, Cellular Movement	30

Top Diseases and Bio Functions

Diseases and Disorders

Name	p-value	# Molecules
Hematological Disease	1.20E-05 - 2.61E-02	22
Immunological Disease	1.20E-05 - 2.54E-02	22
Infectious Disease	1.20E-05 - 2.54E-02	11
Cancer	1.31E-04 - 2.61E-02	61
Inflammatory Disease	1.35E-04 - 2.54E-02	25

Molecular and Cellular Functions

Name	p-value	# Molecules
Cellular Assembly and Organization	1.52E-05 - 2.32E-02	14
Cellular Function and Maintenance	3.01E-05 - 2.54E-02	22
Lipid Metabolism	1.78E-04 - 2.54E-02	12
Small Molecule Biochemistry	1.78E-04 - 2.54E-02	23
Vitamin and Mineral Metabolism	1.78E-04 - 1.02E-02	8

Physiological System Development and Function

Name	p-value	# Molecules
Hematological System Development and Function	1.60E-04 - 2.58E-02	24
Tissue Morphology	1.60E-04 - 2.54E-02	24
Connective Tissue Development and Function	3.84E-04 - 2.54E-02	11
Immune Cell Trafficking	9.61E-04 - 2.08E-02	14
Tissue Development	9.61E-04 - 2.58E-02	24

Top Canonical Pathways

Name	p-value	Ratio
Superpathway of Cholesterol Biosynthesis	1.59E-05	4/87 (0.046)
Role of PI3K/AKT Signaling in the Pathogenesis of Influenza	2.04E-05	5/76 (0.066)
IL-9 Signaling	6.94E-04	3/40 (0.075)
Cholesterol Biosynthesis I	1.95E-03	2/40 (0.05)
Cholesterol Biosynthesis II (via 24,25-dihydrolanosterol)	1.95E-03	2/40 (0.05)

Top Molecules

Other up-regulated

Molecules	Exp. Value	Exp. Chart
TWISTNB	↑12.584	
TMEM68	↑7.233	
PARVG	↑6.500	
TNFAIP3	↑4.829	
MARCO	↑4.728	
CSE1L	↑4.175	
NDST1	↑3.658	
KLF7	↑3.476	
AMMECR1L	↑3.418	
C17orf62	↑3.356	

Other down-regulated

Molecules	Exp. Value	Exp. Chart

Top Upstream Regulators

Upstream Regulator	p-value of overlap	Predicted Activation State
TGFB1	7.23E-07	Activated
PDGF BB	3.70E-06	
TP53	7.82E-06	
AGT	8.64E-06	Activated
CYP51A1	3.31E-05	

Top My Lists

Name	p-value	Ratio

Top My Pathways

Name	p-value	Ratio

Top Tox Lists

Name	p-value	Ratio
Cholesterol Biosynthesis	6.94E-05	3/16 (0.188)
Hepatic Stellate Cell Activation	7.56E-04	3/35 (0.086)
Reversible Glomerulonephritis Biomarker Panel (Rat)	8.38E-03	2/27 (0.074)
Protection from Hypoxia-induced Renal Ischemic Injury (Rat)	2.03E-02	1/4 (0.25)
LXR/RXR Activation	2.53E-02	3/123 (0.024)

Top Tox Functions

Cardiotoxicity

Name	p-value	# Molecules
Cardiac Arrythmia	2.63E-03 - 1.65E-01	4
Pulmonary Hypertension	1.02E-02 - 1.73E-01	1
Cardiac Inflammation	1.70E-02 - 7.89E-02	2
Cardiac Hypoplasia	2.03E-02 - 2.03E-02	1
Cardiac Infarction	3.45E-02 - 6.35E-02	3

Hepatotoxicity

Name	p-value	# Molecules
Liver Inflammation/Hepatitis	3.27E-03 - 2.11E-01	4
Liver Hyperplasia/Hyperproliferation	8.09E-03 - 4.55E-02	9
Liver Steatosis	1.26E-02 - 1.26E-02	5
Hepatocellular Carcinoma	4.55E-02 - 4.55E-02	6
Liver Cirrhosis	5.68E-02 - 3.84E-01	3

Nephrotoxicity

Name	p-value	# Molecules
Renal Inflammation	1.35E-04 - 1.25E-01	8
Renal Nephritis	1.35E-04 - 1.25E-01	8
Renal Necrosis/Cell Death	4.65E-03 - 3.80E-01	5
Renal Atrophy	5.61E-03 - 1.07E-01	2
Renal Dilation	4.52E-02 - 4.52E-02	1

Network 1 : ntpsig_noPdgfb_WT_vs_KO_cv0.1_cmsTp100_direction_corrected - 2013-11-15 07:31 AM : ntpsig_noPdgfb_WT_vs_KO_cv0.1_cmsTp100_direction_corrected : ntpsig_noPdgfb_WT_vs_KO_cv0.1_cmsTp100_direction_corrected - 2013-11-15 07:31 AM

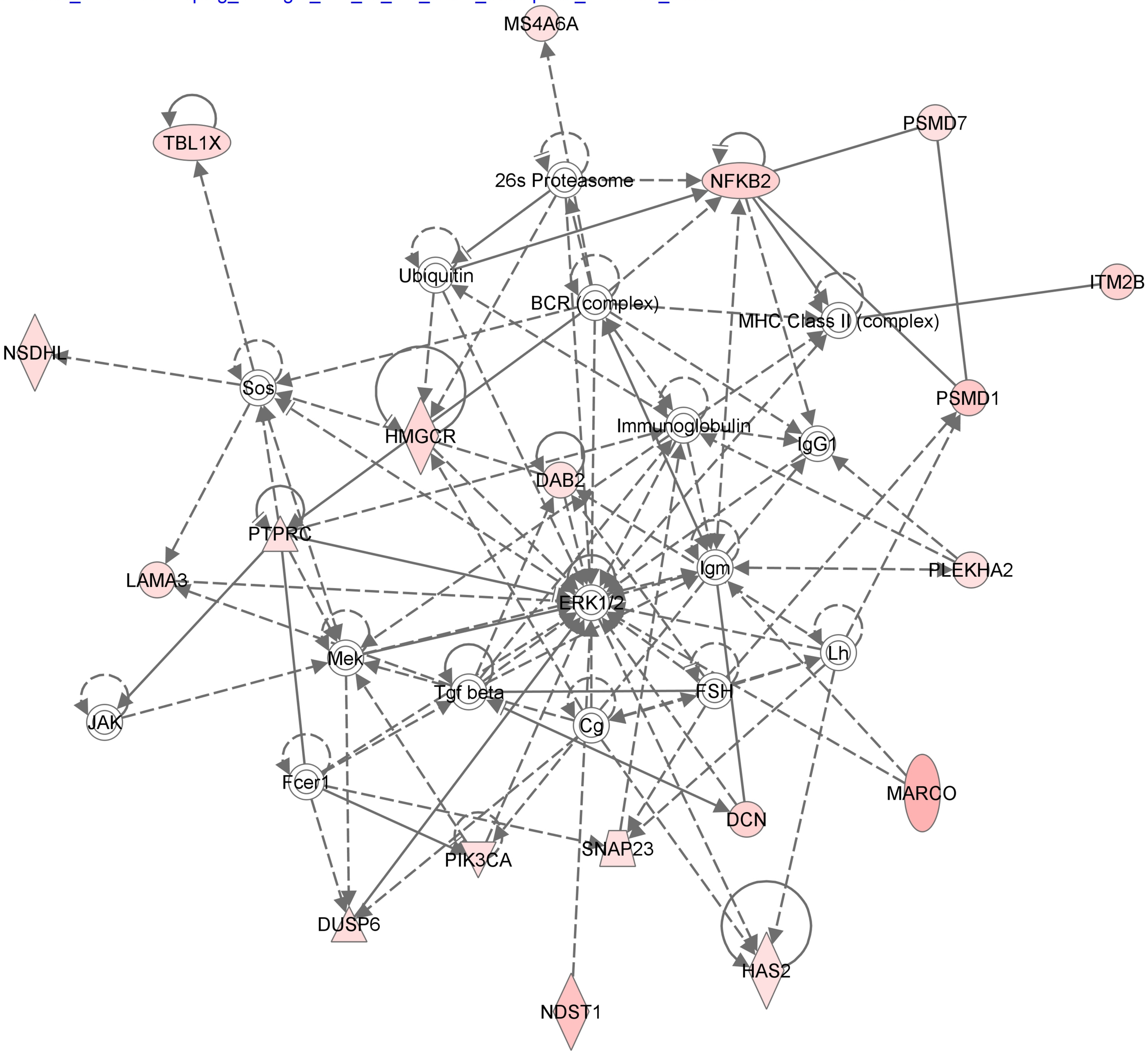

Network 2 : ntpsig_noPdgfb_WT_vs_KO_cv0.1_cmsTp100_direction_corrected - 2013-11-15 07:31 AM : ntpsig_noPdgfb_WT_vs_KO_cv0.1_cmsTp100_direction_corrected : ntpsig_noPdgfb_WT_vs_KO_cv0.1_cmsTp100_direction_corrected - 2013-11-15 07:31 AM

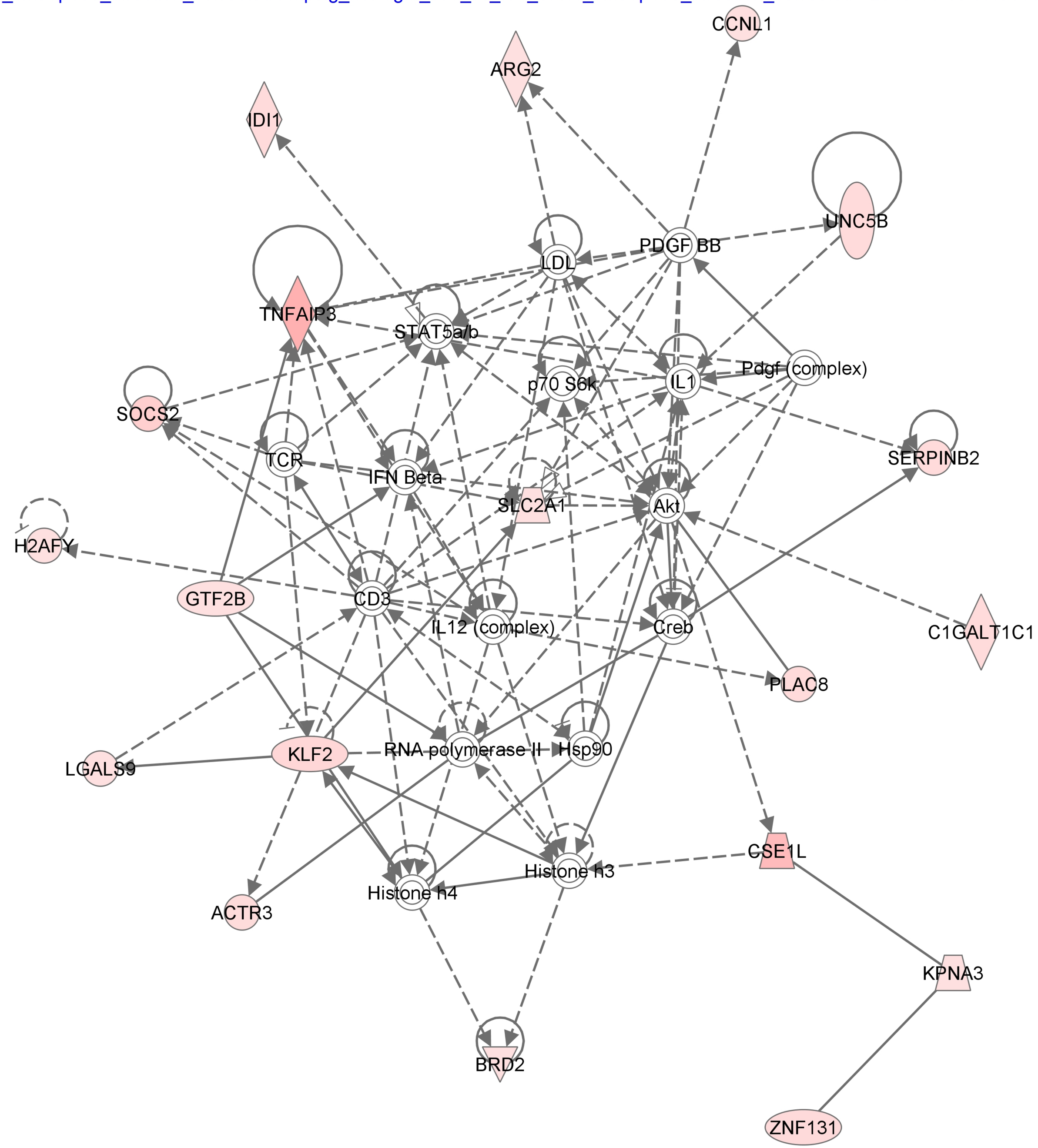

Network 3 : ntpsig_noPdgfb_WT_vs_KO_cv0.1_cmsTp100_direction_corrected - 2013-11-15 07:31 AM : ntpsig_noPdgfb_WT_vs_KO_cv0.1_cmsTp100_direction_corrected : ntpsig_noPdgfb_WT_vs_KO_cv0.1_cmsTp100_direction_corrected - 2013-11-15 07:31 AM

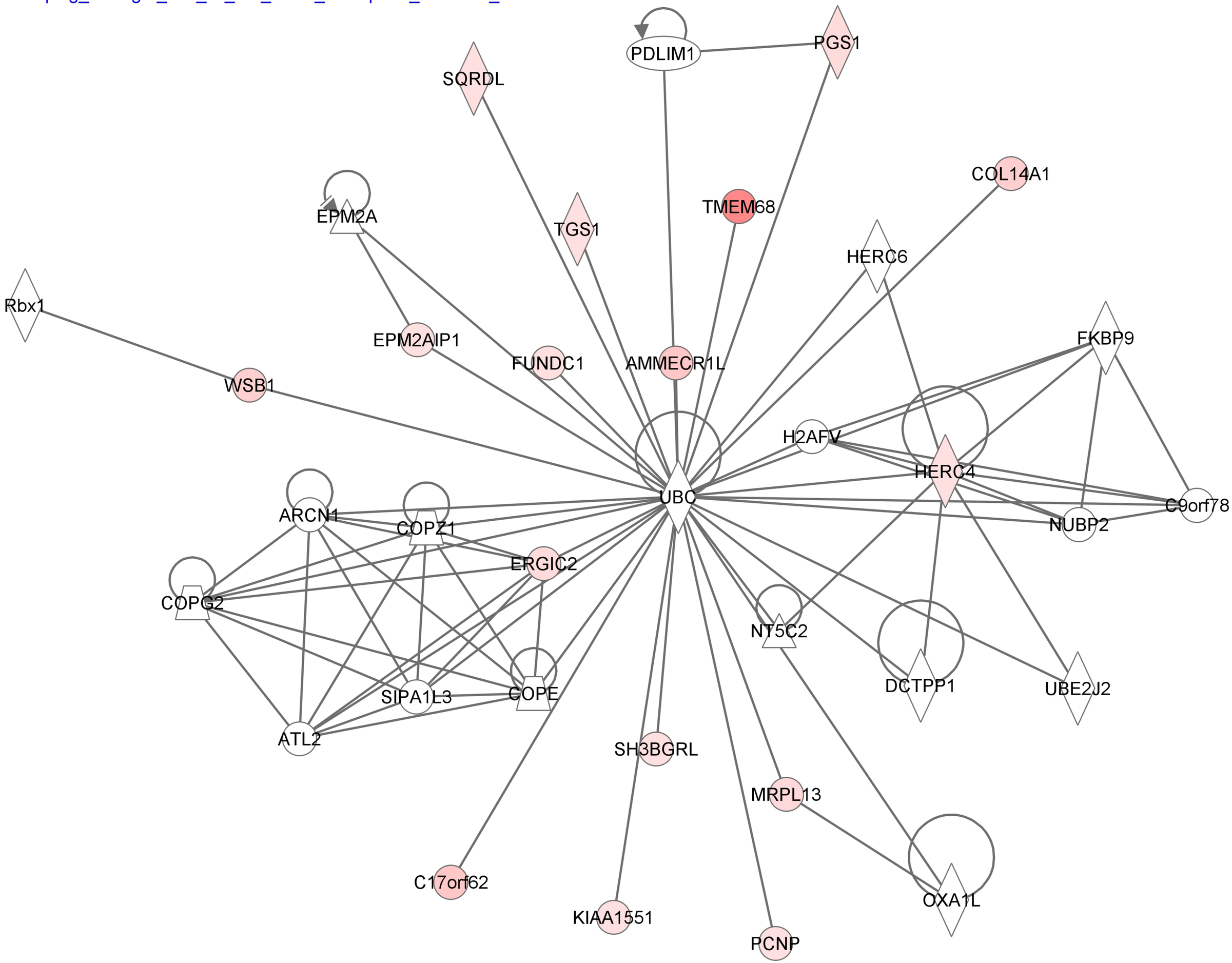

Network 4 : ntpsig_noPdgfb_WT_vs_KO_cv0.1_cmsTp100_direction_corrected - 2013-11-15 07:31 AM : ntpsig_noPdgfb_WT_vs_KO_cv0.1_cmsTp100_direction_corrected : ntpsig_noPdgfb_WT_vs_KO_cv0.1_cmsTp100_direction_corrected - 2013-11-15 07:31 AM

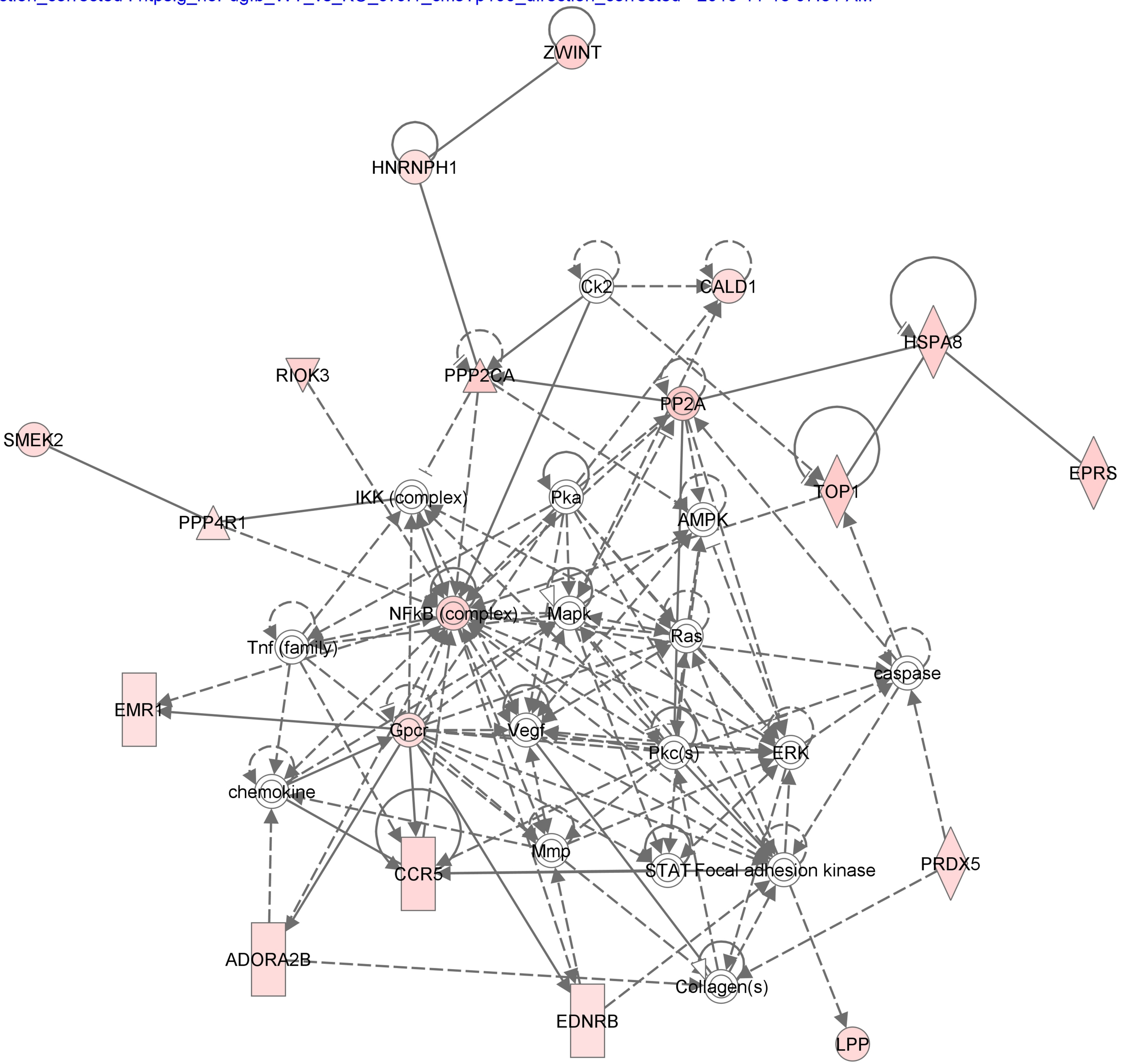

Network 5 : ntpsig_noPdgfb_WT_vs_KO_cv0.1_cmsTp100_direction_corrected - 2013-11-15 07:31 AM : ntpsig_noPdgfb_WT_vs_KO_cv0.1_cmsTp100_direction_corrected : ntpsig_noPdgfb_WT_vs_KO_cv0.1_cmsTp100_direction_corrected - 2013-11-15 07:31 AM

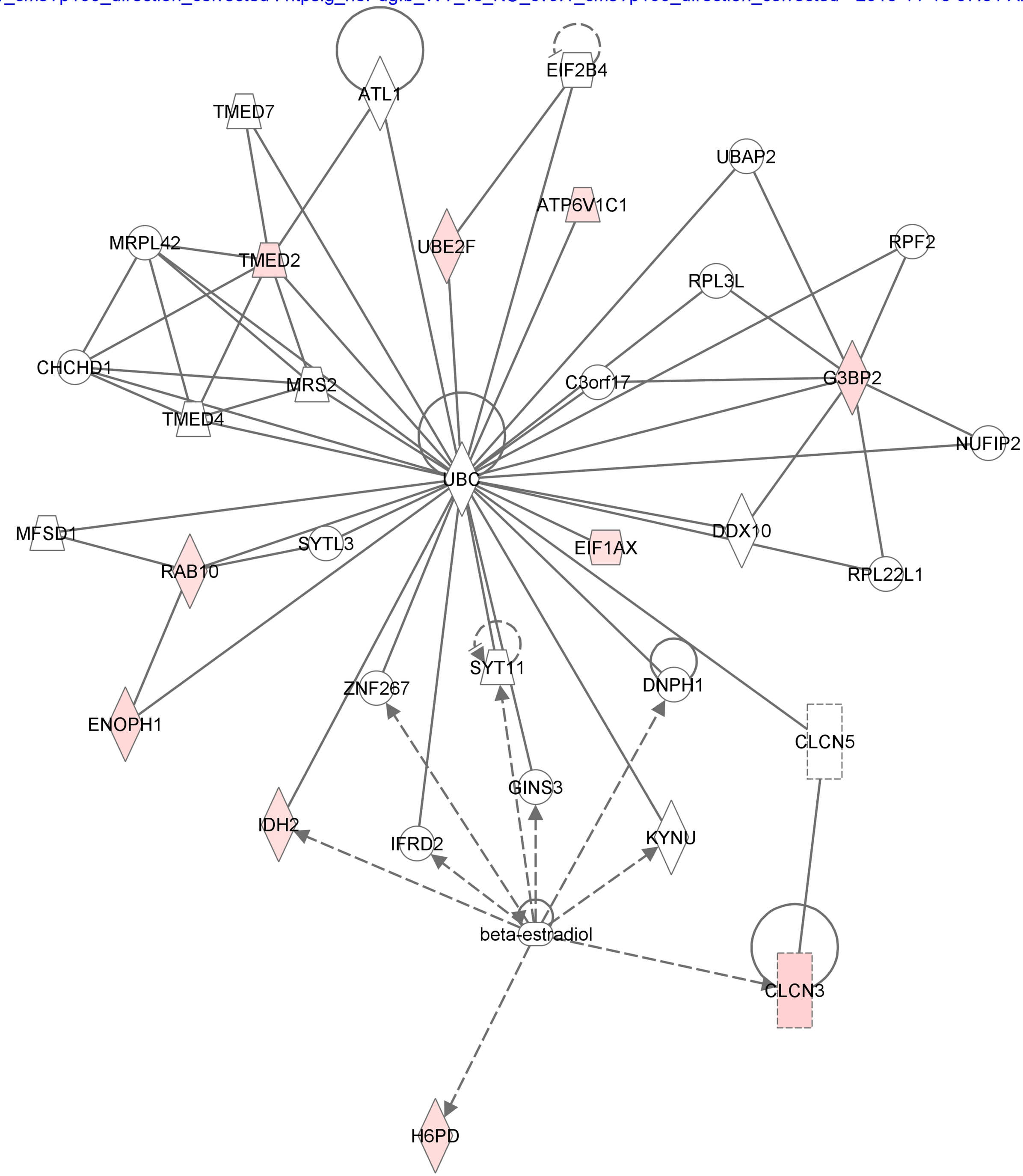

Supplementary table 5

Ingenuity pathway analysis for overexpressed genes in Pdgfrb-wild type hepatic stellate cells compared to knockout with Pdgfb treatment.

Analysis Name: ntpsig_withPdgfb_WT_vs_KO_cv0 - 2013-11-15 08:23 AM
Analysis Creation Date: 2013-11-15
Build version: 242990
Content version: 17199142 (Release Date: 2013-09-17)

Analysis settings

View

Reference set: Ingenuity Knowledge Base (Genes Only)
Relationship to include: Direct and Indirect
Includes Endogenous Chemicals
Optional Analyses: My Pathways My List

Filter Summary:
Consider only relationships where
confidence = Experimentally Observed
Cutoff:

Top Networks

ID	Associated Network Functions	Score
1	Cellular Development, Cellular Growth and Proliferation, Hematological System Development and Function	39
2	Cellular Movement, Hereditary Disorder, Ophthalmic Disease	30
3	Gene Expression, Cell-mediated Immune Response, Cellular Development	29
4	Neurological Disease, Psychological Disorders, Developmental Disorder	28

Top Diseases and Bio Functions

Diseases and Disorders

Name	p-value	# Molecules
Renal and Urological Disease	1.04E-04 - 1.05E-02	15
Inflammatory Response	2.21E-04 - 1.02E-02	22
Immunological Disease	3.35E-04 - 1.25E-02	13
Inflammatory Disease	3.35E-04 - 1.02E-02	11
Neurological Disease	3.35E-04 - 1.02E-02	16

Molecular and Cellular Functions

Name	p-value	# Molecules
Cellular Development	2.08E-05 - 1.20E-02	35
Cellular Growth and Proliferation	2.08E-05 - 1.20E-02	38
Cell-To-Cell Signaling and Interaction	1.34E-04 - 1.17E-02	15
Cellular Compromise	1.34E-04 - 1.10E-02	10
Cellular Function and Maintenance	1.34E-04 - 1.17E-02	18

Physiological System Development and Function

Name	p-value	# Molecules
Tumor Morphology	2.08E-05 - 1.02E-02	10
Nervous System Development and Function	2.60E-05 - 1.23E-02	16
Tissue Development	2.60E-05 - 1.24E-02	22
Hair and Skin Development and Function	7.76E-05 - 1.03E-02	10
Hematological System Development and Function	1.04E-04 - 1.24E-02	31

Top Canonical Pathways

Name	p-value	Ratio
Actin Nucleation by ARP-WASP Complex	2.96E-03	3/67 (0.045)
Regulation of Cellular Mechanics by Calpain Protease	3.12E-03	3/73 (0.041)
Protein Kinase A Signaling	3.36E-03	7/407 (0.017)
Integrin Signaling	3.43E-03	5/208 (0.024)
FAK Signaling	1.01E-02	3/106 (0.028)

Top Molecules

Other up-regulated

Molecules	Exp. Value	Exp. Chart
TWISTNB	8.264	
LPP	4.292	
KLF7	4.237	
PARVG	4.122	
KRAS	3.618	
C17orf62	3.591	
IL27RA	3.483	
ITGB1	3.297	
PKIG	3.113	
RFT1	2.996	

Other down-regulated

Molecules	Exp. Value	Exp. Chart

Top Upstream Regulators

Upstream Regulator	p-value of overlap	Predicted Activation State
TP53	6.71E-06	Activated
TGFB1	7.98E-06	
Salmonella enterica serotype abortus equi lipopolysaccharide	2.14E-05	Activated
PDGF BB	2.47E-05	
lipopolysaccharide	2.70E-05	Activated

Top My Lists

Name	p-value	Ratio

Top My Pathways

Name	p-value	Ratio

Top Tox Lists

Name	p-value	Ratio
Hepatic Fibrosis	1.32E-02	3/96 (0.031)
Cell Cycle: G1/S Checkpoint Regulation	4.39E-02	2/65 (0.031)
Liver Necrosis/Cell Death	4.57E-02	4/262 (0.015)
Aryl Hydrocarbon Receptor Signaling	4.91E-02	3/160 (0.019)
Genes Upregulated in Response to Proteinuria-induced Oxidative Stress in Renal Proximal Tubule Cells (Human)	5.01E-02	1/10 (0.1)

Top Tox Functions

Assays: Clinical Chemistry and Hematology

Name	p-value	# Molecules
Increased Levels of Red Blood Cells	9.00E-02 - 9.00E-02	2
Increased Levels of Alkaline Phosphatase	2.99E-01 - 2.99E-01	1

Cardiotoxicity

Name	p-value	# Molecules
Congenital Heart Anomaly	6.66E-03 - 2.19E-01	2
Cardiac Fibrosis	9.30E-02 - 9.30E-02	1
Cardiac Hypoplasia	1.07E-01 - 1.07E-01	1
Cardiac Arrythmia	1.13E-01 - 3.84E-01	2
Tachycardia	1.25E-01 - 1.25E-01	1

Hepatotoxicity

Name	p-value	# Molecules
Liver Inflammation/Hepatitis	5.12E-03 - 1.70E-01	3
Hepatocellular Carcinoma	1.02E-02 - 4.82E-01	3
Liver Hyperplasia/Hyperproliferation	1.02E-02 - 4.82E-01	5
Liver Damage	2.03E-02 - 1.29E-01	2
Liver Hypoplasia	2.05E-02 - 2.05E-02	2

Nephrotoxicity

Name	p-value	# Molecules

Renal Hydronephrosis	1.04E-04 - 1.04E-04	5
Renal Inflammation	7.97E-04 - 1.12E-01	7
Renal Nephritis	7.97E-04 - 1.12E-01	7
Renal Necrosis/Cell Death	1.04E-03 - 8.37E-02	5
Kidney Failure	5.12E-03 - 2.19E-01	3

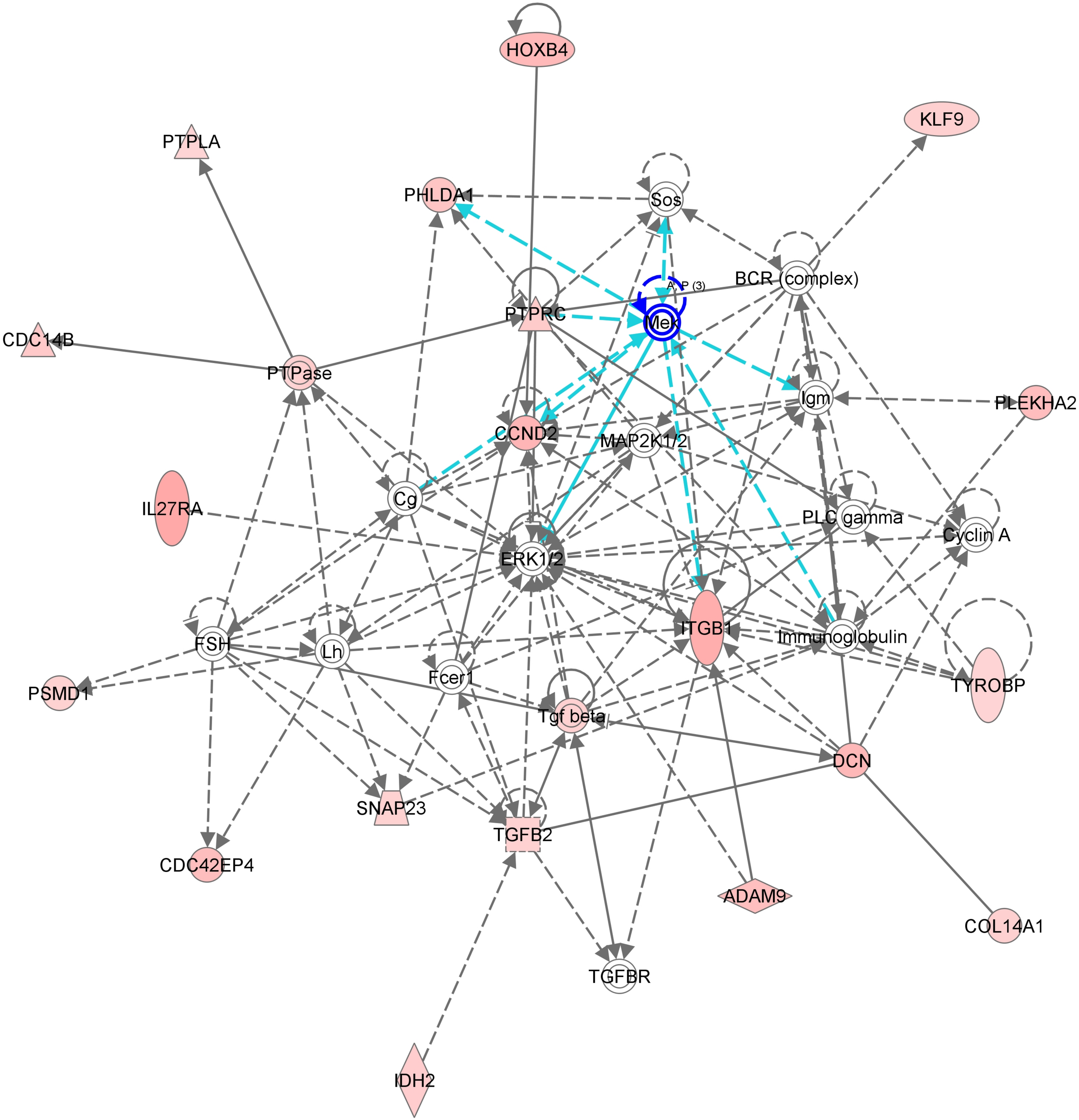

Network 2 : ntpsig_withPdgfb_WT_vs_KO_cv0 - 2013-11-15 08:23 AM : ntpsig_withPdgfb_WT_vs_KO_cv0 : ntpsig_withPdgfb_WT_vs_KO_cv0 - 2013-11-15 08:23 AM

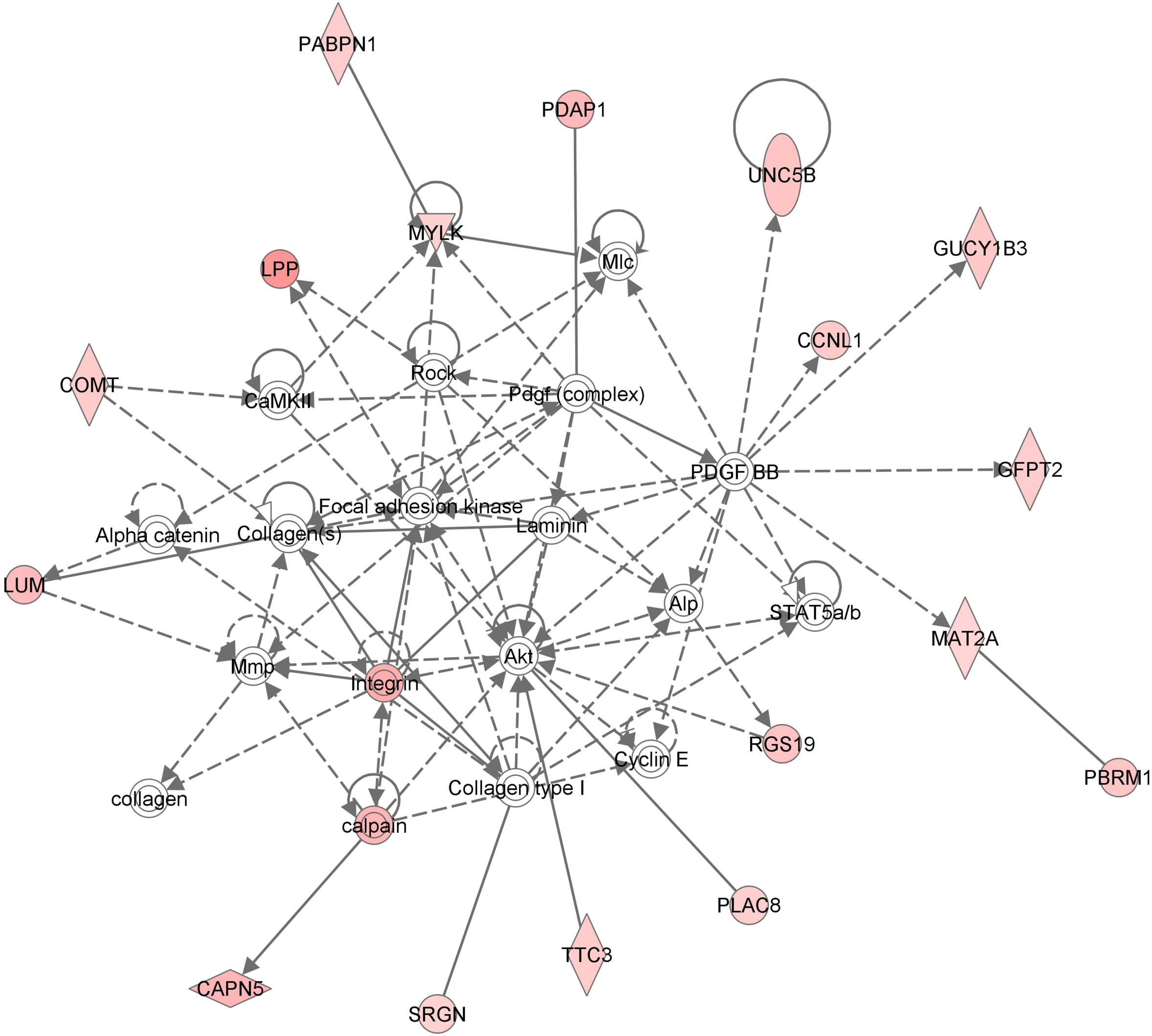

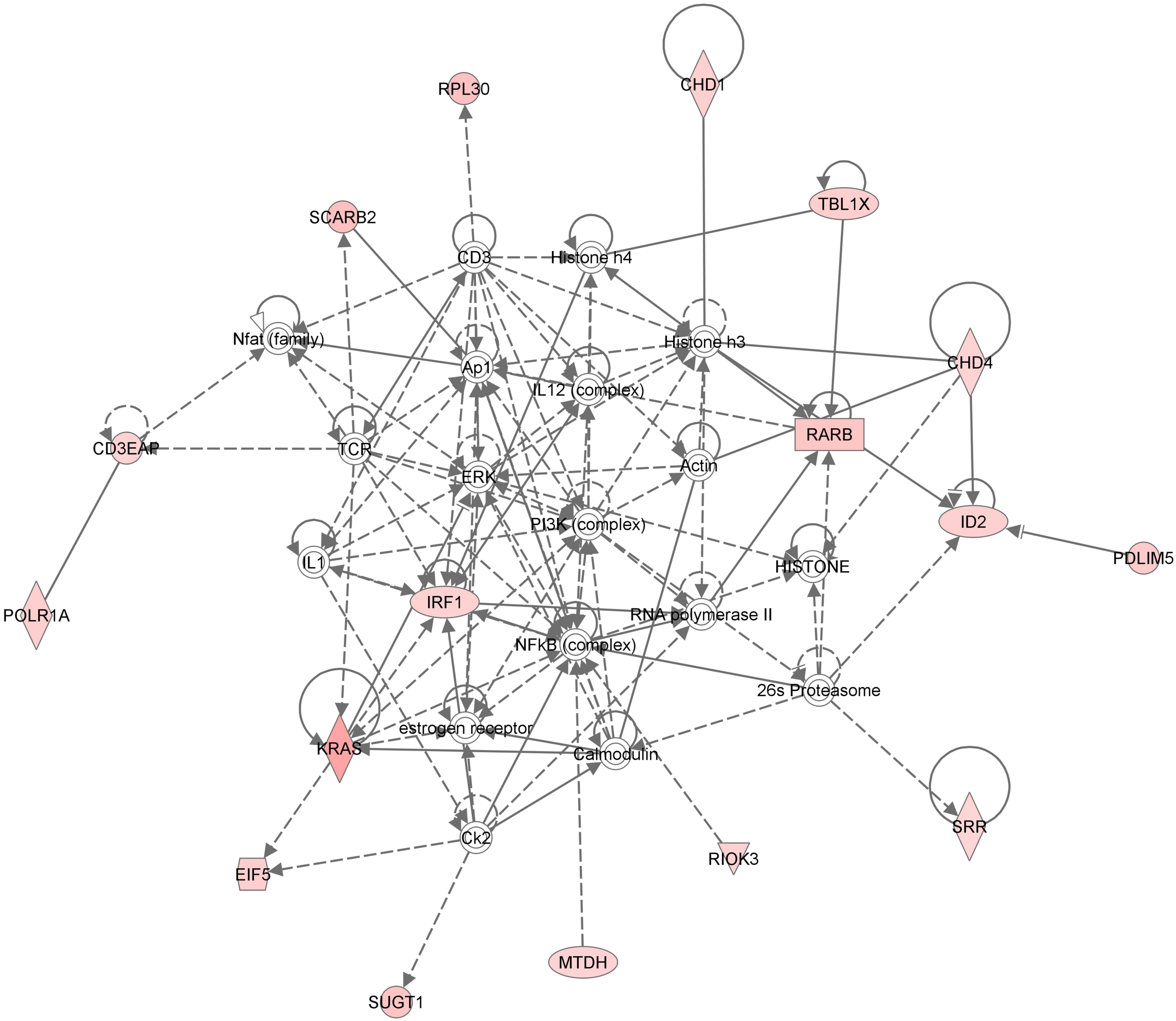

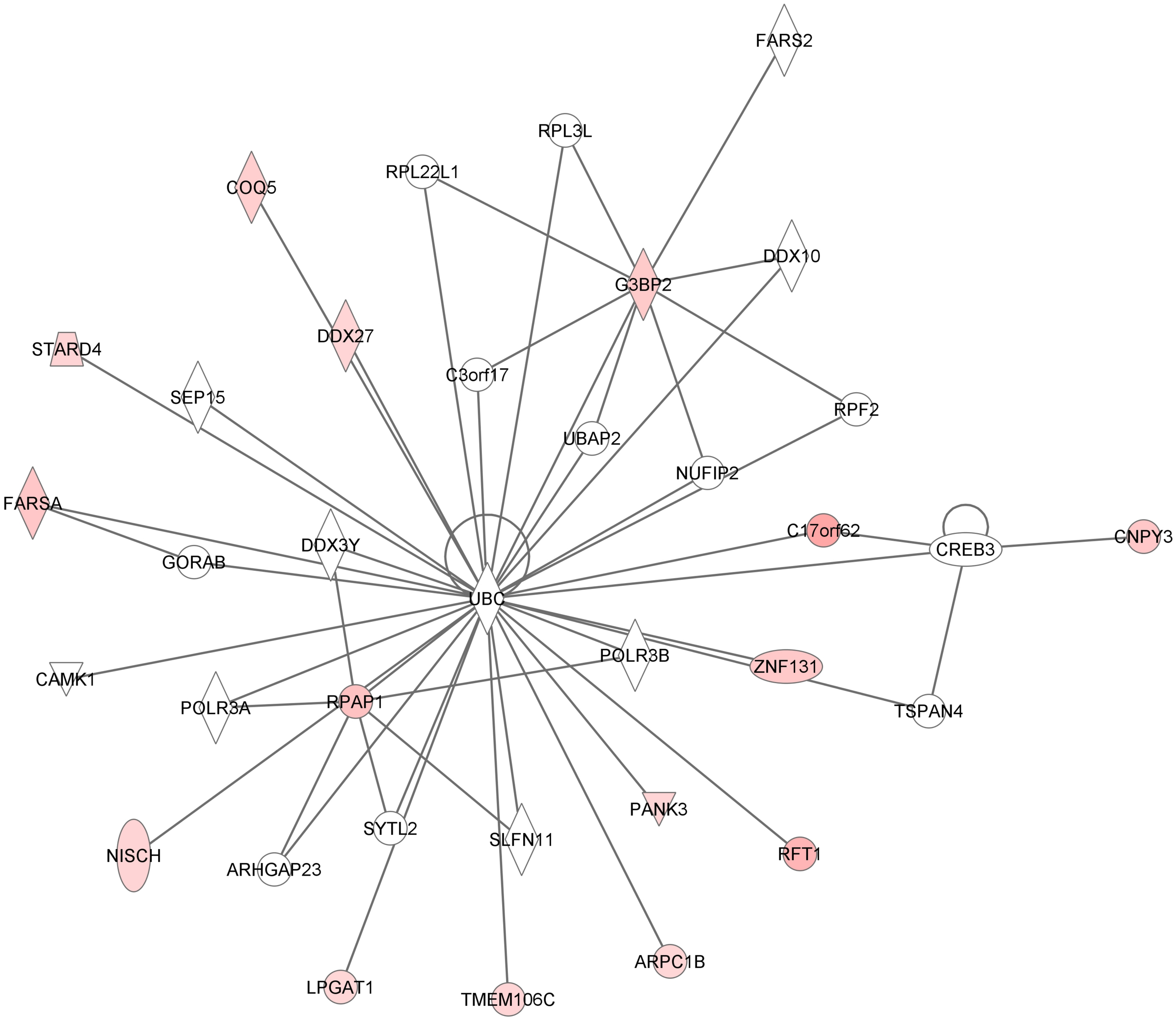

Network 5 : ntpsig_withPdgfb_WT_vs_KO_cv0 - 2013-11-15 08:23 AM : ntpsig_withPdgfb_WT_vs_KO_cv0 : ntpsig_withPdgfb_WT_vs_KO_cv0 - 2013-11-15 08:23 AM

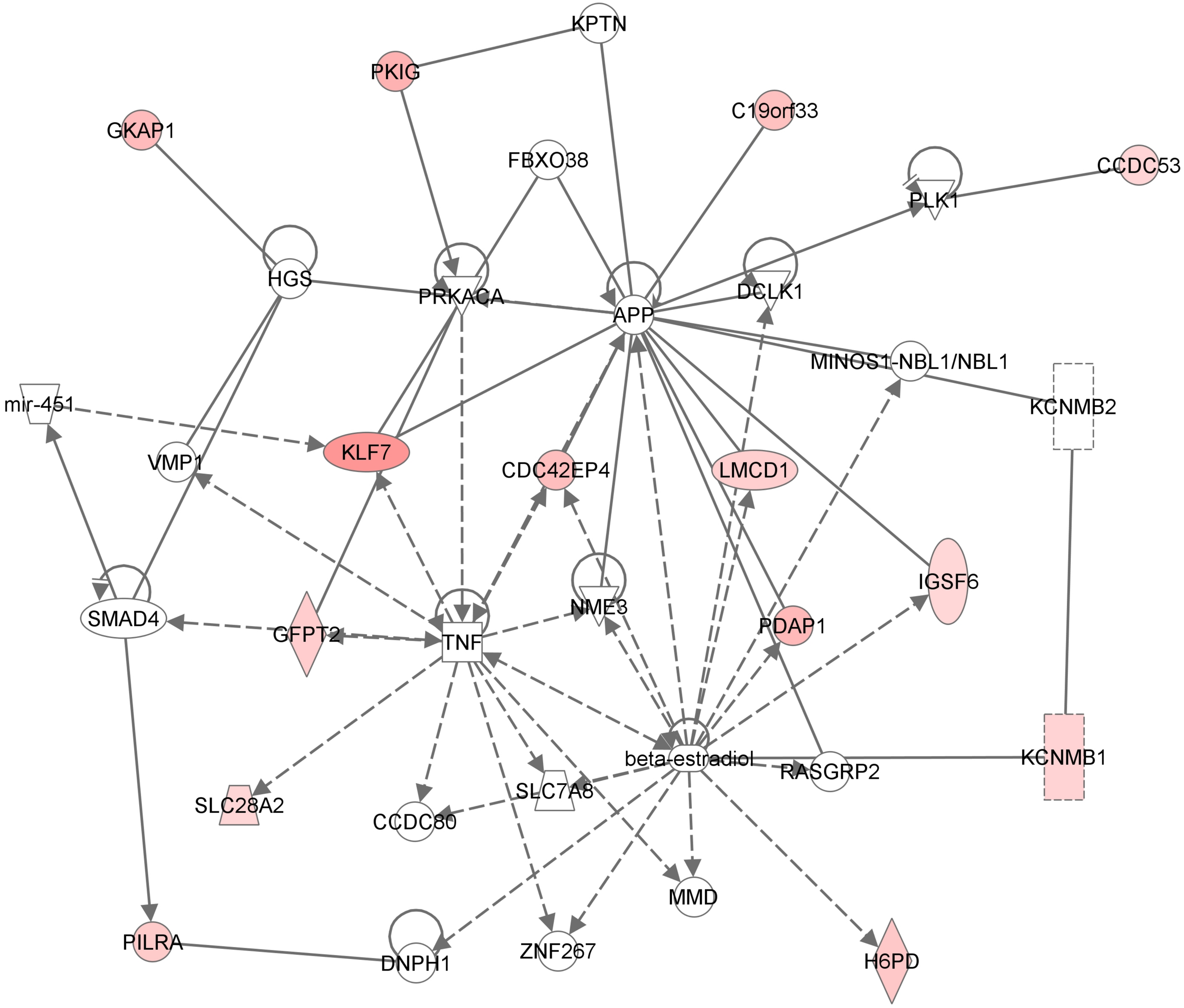

Supplementary figure legends

Supplementary Fig. 1. Generation of a knock down of β-PDGFR in hepatic stellate cells and induction of acute and chronic liver injury using CCl_4.

(A) Schematic diagram of mice with an hepatic stellate cell-specific knock down of β-PDGFR. β-PDGFR$^{fl/fl}$ mice were crossed with a transgenic line expressing Cre recombinase under the control of the glial fibrillary acidic protein (GFAP) promoter (GFAP-Cre) to generate Tg(GFAP-Cre)/+; β-PDGFR$^{fl/fl}$ mice with a stellate cell–specific knock down of β-PDGFR.

(B) Macroscopic images showing mice after treatment with either acute or chronic CCl_4 (or oil control) (magnification 200x). Animals were sacrificed 48 hours following the last injection.

(C) Graph shows liver weight to body weight ratio of each mouse, as well as mean value per experimental group (error bars indicate SEM). There was n difference in liver/body weight ratio after 6 weeks of CCl_4 treatment.

Supplementary Fig. 2. Δβ-PDGFR mice show less necrosis following acute liver injury.

(A) Images show H&E staining of paraffin embedded liver sections following either 1 or 6 weeks of CCl_4 administration (or oil control) (magnification 200x).

(B) Graphs show necrosis and inflammation scores assessed by a blinded pathologist based on severity of the phenotype within H&E stained tissue sections. Decreased areas of necrotic tissue within liver sections were seen after 1 week of CCl_4 treatment within Δβ-PDGFR mice. At least n=3 animals were included for 1 week treatments, and at least n=5 animals were included for 6 weeks of treatment. For each mouse, 5 fields were analyzed and the average was plotted. Mean values are presented per experimental group (error bars indicate SEM).

Supplementary Fig. 3. Δβ-PDGFR mice show diminished expansion of activated hepatic stellate cells upon acute and chronic liver injury.

(A) Images show αSMA staining of paraffin embedded liver sections following 6 weeks of CCl_4 treatment (magnification 200x). The graph shows quantification of αSMA^+ tissue area measured by morphometry. The area of activated HSCs as measured my αSMA expression is lower in Δβ-PDGFR mice after one week of treatment, and reaches a highly significant difference after chronic treatment for six weeks.

(B) Immunoblot demonstrates reduced expression of αSMA and Desmin in whole liver

lysates of Δβ-PDGFR mice (n=4) versus controls (n=3) upon chronic liver injury induced by 6 weeks of CCl_4 administration. The graph shows densitometric analysis of each band, showing a diminished relative expression of αSMA in mice with reduced expression of the receptor compared with controls.

Supplementary Fig. 4. Δβ-PDGFR mice show reduced expression of Desmin on hepatic stellate cells upon acute liver injury.

(A) Images show Desmin staining of paraffin embedded liver sections following 1 week of CCl_4 treatment (magnification 200x). The graph shows percentage of $Desmin^+$ tissue area measured by morphometry. The area of Desmin-positive HSC expansion in the liver as measured my immunohistochemistry is significantly lower in Δβ-PDGFR mice after one week of treatment.

Supplementary Fig. 5. Δβ-PDGFR mice do not exhibit significantly less hepatic injury upon ligation of the common bile duct.

Δβ-PDGFR and control mice underwent either sham laparotomy or ligation of the common bile duct. Mice were sacrificed 14 days post surgery.

(A) Sirius Red staining of paraffin embedded liver sections after two weeks of either sham laparotomy or ligation of the common bile duct (BDL).

(B) Graph shows the percentage of Sirius Red staining measured by morphometry. The area of fibrotic tissue is lower yet not significantly reduced within Δβ-PDGFR animals versus controls (magnification 200x).

(C) Levels of serum AST and ALT during acute and chronic injury.

All figures represent the mean of at least n=4 animals per experimental group (error bars indicate SEM).

Supplementary Fig. 6. Primary Stellate cells of Δβ-PDGFR mice have reduced proliferation upon injury *in vivo.*

Groups of mice were injected with CCl_4 over one week. Forty four hours after the last CCl_4 injection, mice were injected with BrdU. Stellate cells were isolated 4 hours later and stained for CD45 and BrdU.

(A) Flow cytrometric analysis for CD45 expression was used to purify the cell suspension, followed by detection of UV-autofluorescence and expression of BrdU to quantify the

percentage of proliferating HSCs (44.3% in β-PDGFR stellate cells; 16.3% in Δβ-PDGFR stellate cells).
(B) Flow cytometric analysis of primary HSCs shows increased proliferation of control HSCs upon injury compared to cells lacking β-PDGFR.
Data represent the mean value of 3 separate experiments, each including n=3 animals per group (*p<0.05, error bars indicate SEM).

Supplementary Fig. 7. Generation of an hepatic stellate cell-specific auto-activating mutant of β-PDGFR and effects of acute and chronic CCl_4 liver injury.
(A) Schematic depicting of the generation of an hepatic stellate cell-specific auto-activating mutant of β-PDGFR. β-PDGFR$^{+/betaJ}$ mice were crossed with a transgenic line expressing Cre recombinase under the control of the glial fibrillary acidic protein (GFAP) promoter (GFAP-Cre) to generate β-PDGFR$^{+/betaJ}$; Tg(GFAP-Cre)/+ mice with a stellate cell–specific auto-activation of β-PDGFR.
(B) Macroscopic images showing mice of both groups after either treatment 6 weeks CCl_4 (or oil control).
(C) Graph shows liver weight to body weight ratio of each mouse, as well as mean value per experimental group (error bars indicate SEM). There was no difference in liver/body weight ratio after 1 or 6 weeks of CCl_4. At least n=3 mice were included in the acute treatment group and at least n=5 mice were included in the chronic treatment group.
(D) Graph shows time course of serum transaminase levels without treatment and following 1 or 6 weeks of CCl_4. Both groups respond to treatment with an increase in serum transaminase levels, yet no difference could be assessed between both genotypes.

Supplementary Fig. 8. Acute and chronic treatment with CCl_4 leads to increased areas of necrosis and inflammation in both βJ and control mouse livers.
(A) Images demonstrate H&E staining of paraffin embedded liver sections following injection with oil over 1 week or either 1 or 6 week injections with CCl_4 (magnification 200x).
(B) Graphs show necrosis and inflammation scores assessed by a blinded pathologist based on severity of the phenotype within H&E stained tissue sections. Increased areas of necrotic tissue within liver sections were seen after 1 and 6 weeks of CCl_4 in both βJ and control mice. At least n=3 animals were included for 1 week CCl_4, and at least n=4 animals were included for 6 weeks of CCl_4. For each mouse, 5 fields were analyzed and the average was plotted. Mean values are presented per experimental group (error bars indicate SEM).

Supplementary Fig. 9. Knock down of β-PDGFR on HSCs does not protect from formation of dysplastic nodules upon long-term injury.

(A) Schematic depicting of the induction of long-term liver injury: Mice were administered a single dose of DEN at day 15, followed by weekly injections of CCl_4 beginning at day 28. After 22 CCl_4 injections, mice were sacrificed 48 hours following the last injection.

(B) Macroscopic images showing increased nodule formation after long-term injury within both Δβ-PDGFR mice and the control group.

(C) The graph shows liver weight to body weight ratio for each mouse. There was an increase in liver to body weight ratio for both Δβ-PDGFR and control mice. Mean and SEM were shown for each experimental group. At least n=5 mice were included per group.

(D) The graph shows the diameter of the largest tumor per mouse per experimental group. There was no significant difference in tumor diameter within the groups. Mean values are presented per group (error bars indicate SEM).

(E) The graph shows the average tumor diameter of each mouse per experimental group. There was no difference in average tumor diameter within the investigated groups. Mean and SEM were shown for each experimental group.

(F) The images show H&E staining of paraffin embedded liver sections. Dysplastic nodules could be detected in both Δβ-PDGFR and control mice, with no sign for definite malignancy or difference in stage of atypia (40x magnification, inset shows 100x magnification).

(G) Whole liver mRNA expression of *Collagen α1(I)* after DEN and CCl_4 treatment shows reduced expression within the Δβ-PDGFR group versus control animals.

All figures represent the mean of at least n=5 animals per experimental group. mRNA is expressed normalized to *Gapdh* (error bars indicate SEM).

Supplementary Fig. 10. Constitutive activation of β-PDGFR on HSCs does not increase the development of dysplastic nodules following long-term injury.

Mice were injected with a single dose of DEN at day 15, followed by weekly injections of CCl4 beginning at day 28. After a completion of 22 CCl_4 injections, mice were sacrificed 48 hours following the last injection.

(A) Macroscopic images showing nodule formation after long-term injury in both βJ and control mice.

(B) Graph indicating tumor number of each experimental mouse. There were no differences in appearance of macroscopic nodules on the liver surface between the βJ and control group.

Mean and SEM were shown for each experimental group. At least n=8 mice were included per group.
(C) The graph shows liver weight to body weight ratio for each mouse. There was no difference in liver to body weight ratio between the groups. Mean and SEM were shown for each experimental group.
(D) The graph shows the diameter of the largest tumor per mouse per experimental group. There was no significant difference in tumor diameter within the groups. Mean values are presented per group (error bars indicate SEM).
(E) The graph shows the average tumor diameter of each mouse per experimental group. There was no difference in average tumor diameter within the groups. Mean and SEM were shown for each experimental group.
(F) The images show H&E staining of paraffin embedded liver sections. Dysplastic nodules could be detected in both βJ and control mice, with no sign for definite malignancy or difference in stage of atypia (100x magnification).

Supplementary Fig. 11. Genome-wide expression analysis reveals established targets downstream of β-PDGFR signaling.
Hepatic stellate cells of β-PDGFR and Δβ-PDGFR mice were isolated and either treated with PDGF-B or left untreated. Graphs show Ingenuity pathway analysis of genome-wide expression profiles of primary hepatic stellate cells of either β-PDGFR and Δβ-PDGFR mice.
(A) Comparison of hepatic stellate cells of β-PDGFR and Δβ-PDGFR mice without treatment with PDGF-B.
(B) Comparison of hepatic stellate cells of β-PDGFR and Δβ-PDGFR mice with treatment with PDGF-B.

Supplementary Fig. 12. Genome-wide expression analysis reveals novel targets downstream of β-PDGFR signaling.
Hepatic stellate cells of β-PDGFR and Δβ-PDGFR mice were isolated and either treated with PDGF-B or plain medium. Graphs show GSEA and Ingenuity pathway analysis of genome-wide expression profiles of primary hepatic stellate cells of either β-PDGFR and Δβ-PDGFR mice.
(A) GSEA analysis comparing hepatic stellate cell signatures of β-PDGFR and Δβ-PDGFR mice without treatment with PDGF-B. Genes of the β-PDGFR signature enrich for genes of the IL1R pathway.

(B) GSEA analysis comparing hepatic stellate cell signatures of β-PDGFR and Δβ-PDGFR mice with treatment with PDGF-B. Genes of the β-PDGFR signature show a stronger enrichment for genes of the IL1R pathway.
(C) GSEA analysis comparing hepatic stellate cell signatures of β-PDGFR and Δβ-PDGFR mice without treatment with PDGF-B. Genes of the β-PDGFR signature enrich for genes of the NF-kB pathway.
(D) GSEA analysis comparing hepatic stellate cell signatures of β-PDGFR and Δβ-PDGFR mice with treatment with PDGF-B. Genes of the β-PDGFR signature show a stronger enrichment for genes of the NF-kB pathway.
(E) Ingenuity pathway analysis comparing hepatic stellate cell signatures of β-PDGFR and Δβ-PDGFR mice without treatment with PDGF-B.
(F) Ingenuity pathway analysis comparing hepatic stellate cell signatures of β-PDGFR and Δβ-PDGFR mice with treatment with PDGF-B.

Supplementary figure 1

A

β−PDGFR$^{fl/fl}$ x Tg(GFAP-Cre)/+
Experimental group (Δβ-PDGFR): Tg(GFAP-Cre)/+; β-PDGFR$^{fl/fl}$
Control group (β-PDGFR): β-PDGFR$^{fl/fl}$

B

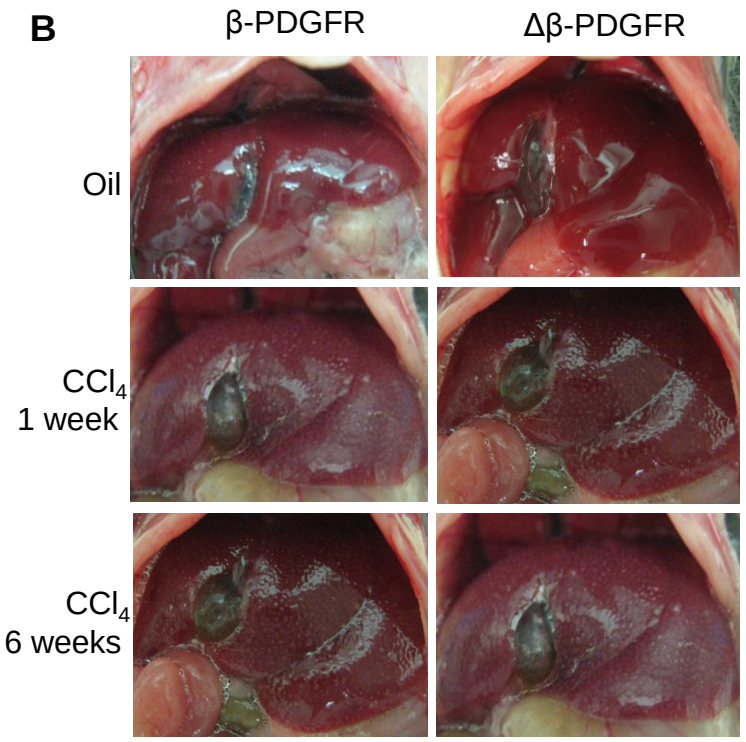

C

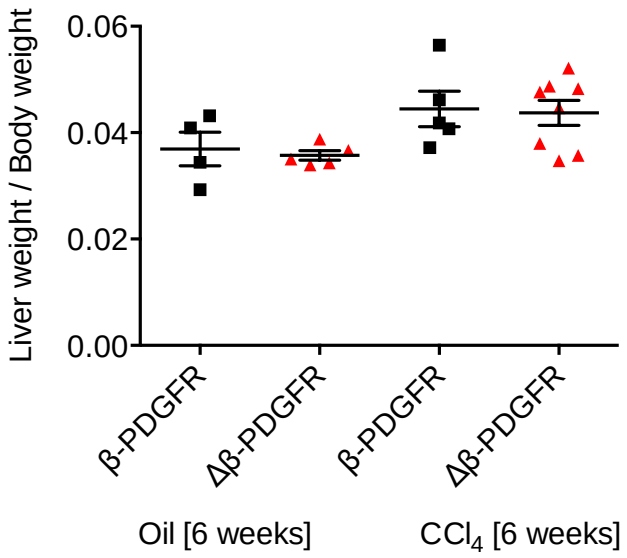

Supplementary figure 2

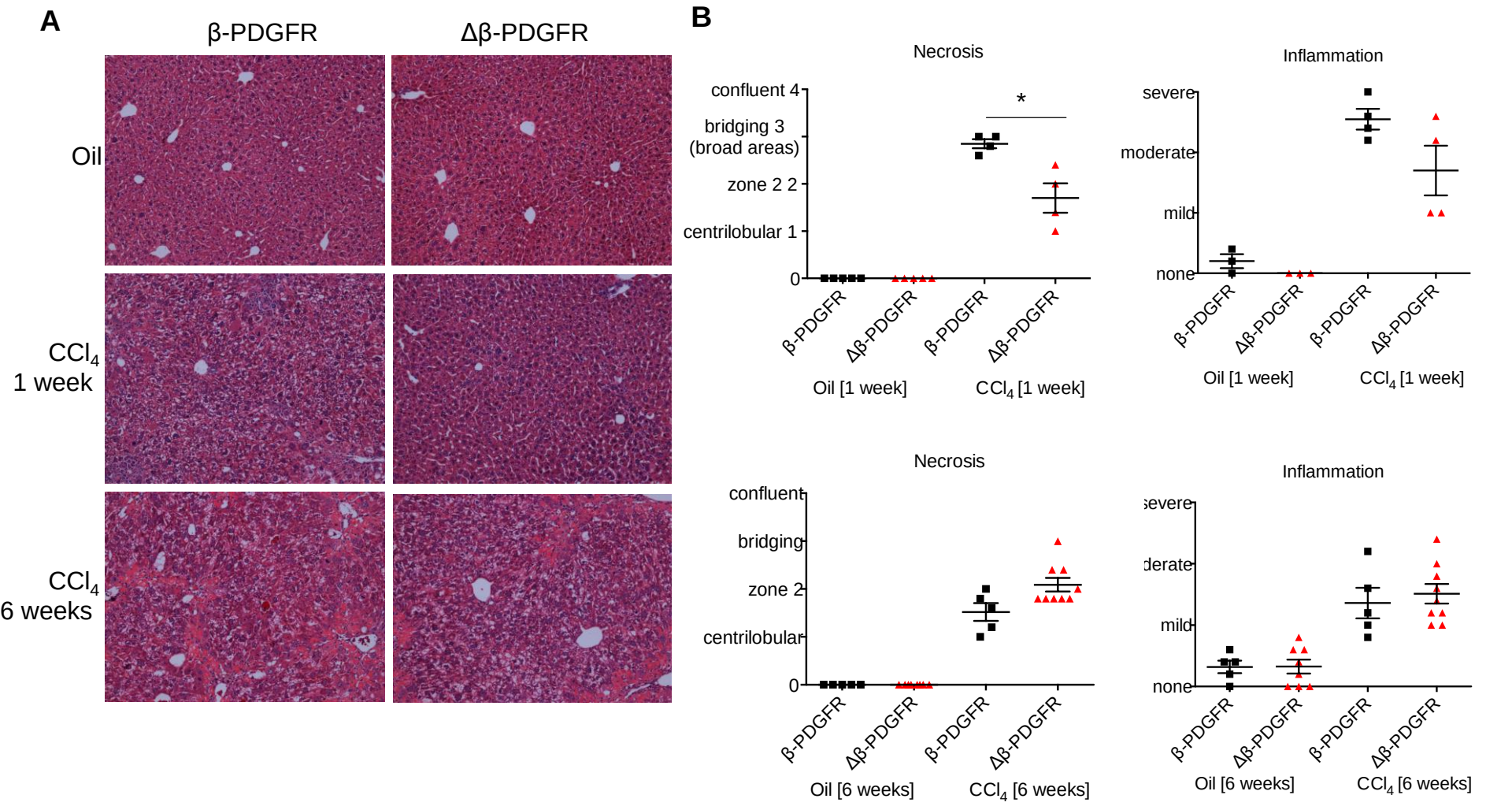

Supplementary figure 3

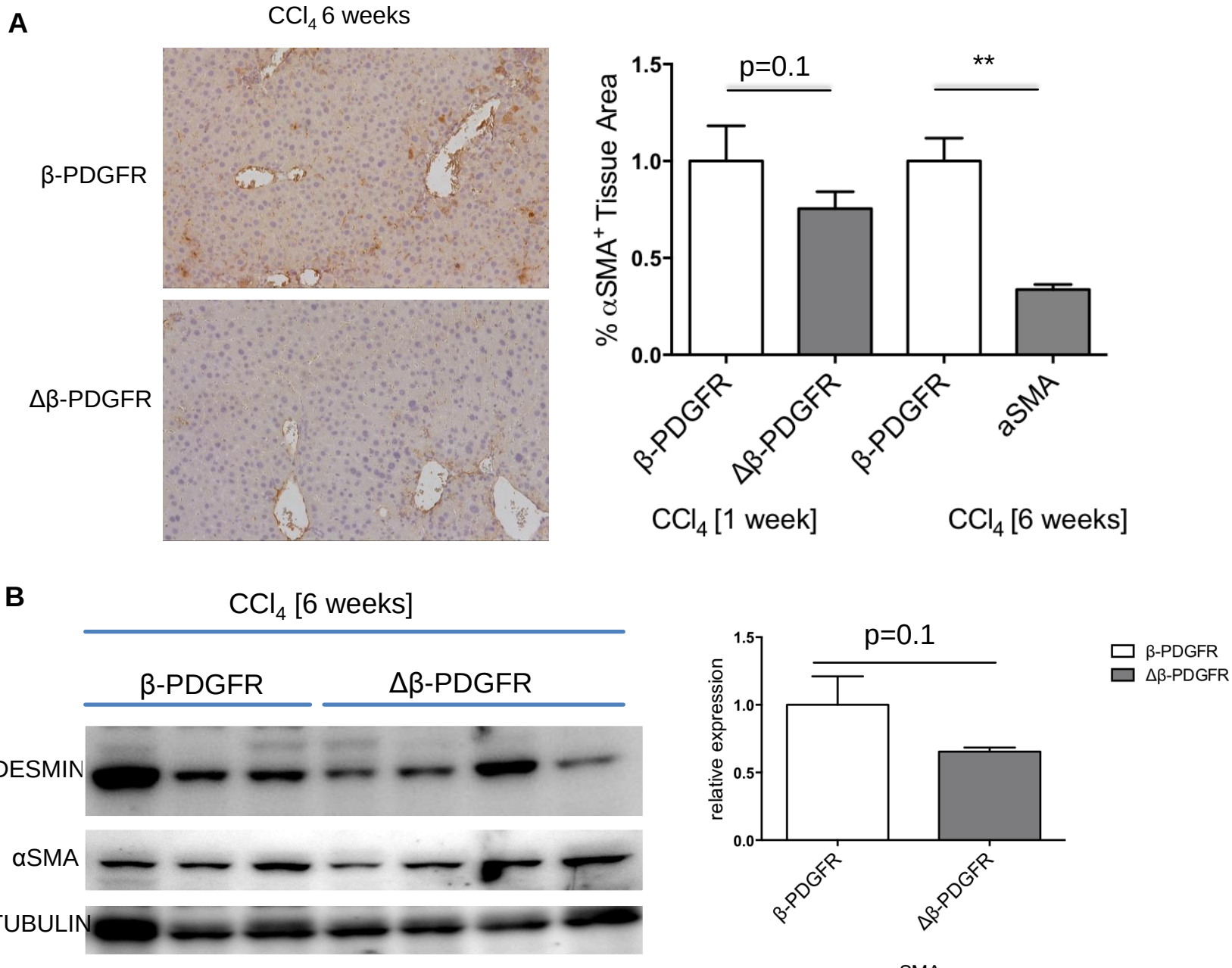

Supplementary figure 4

A

CCl_4 1 week

β-PDGFR

Δβ-PDGFR

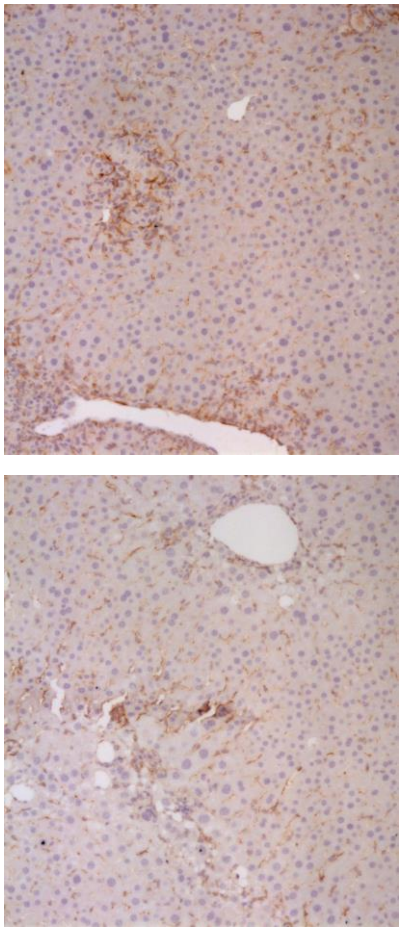

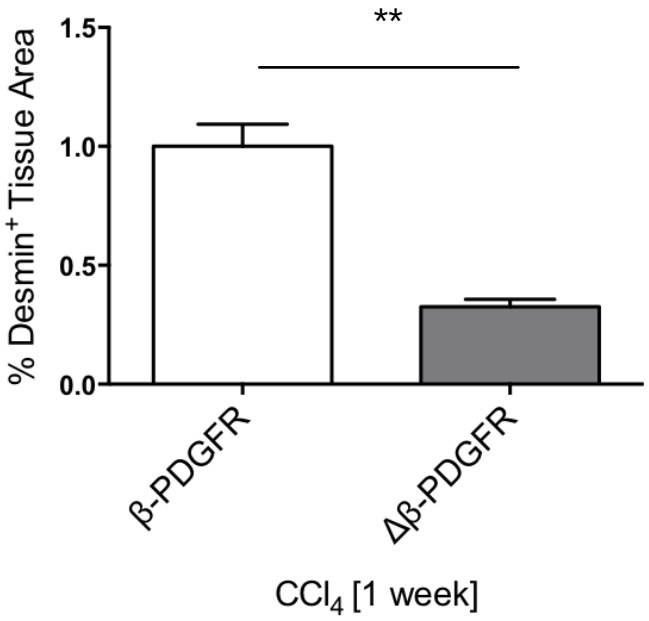

Supplementary figure 5

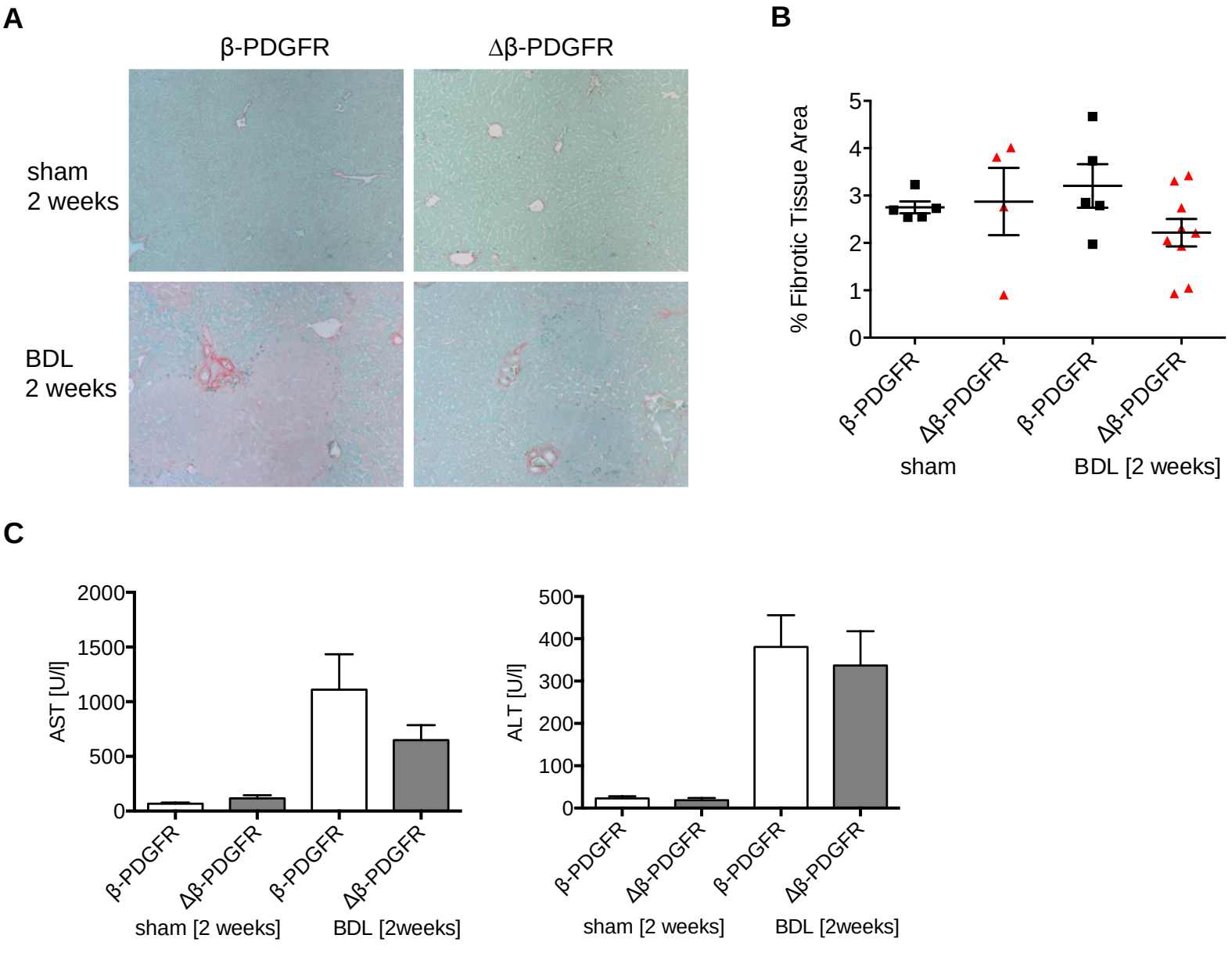

Supplementary figure 6

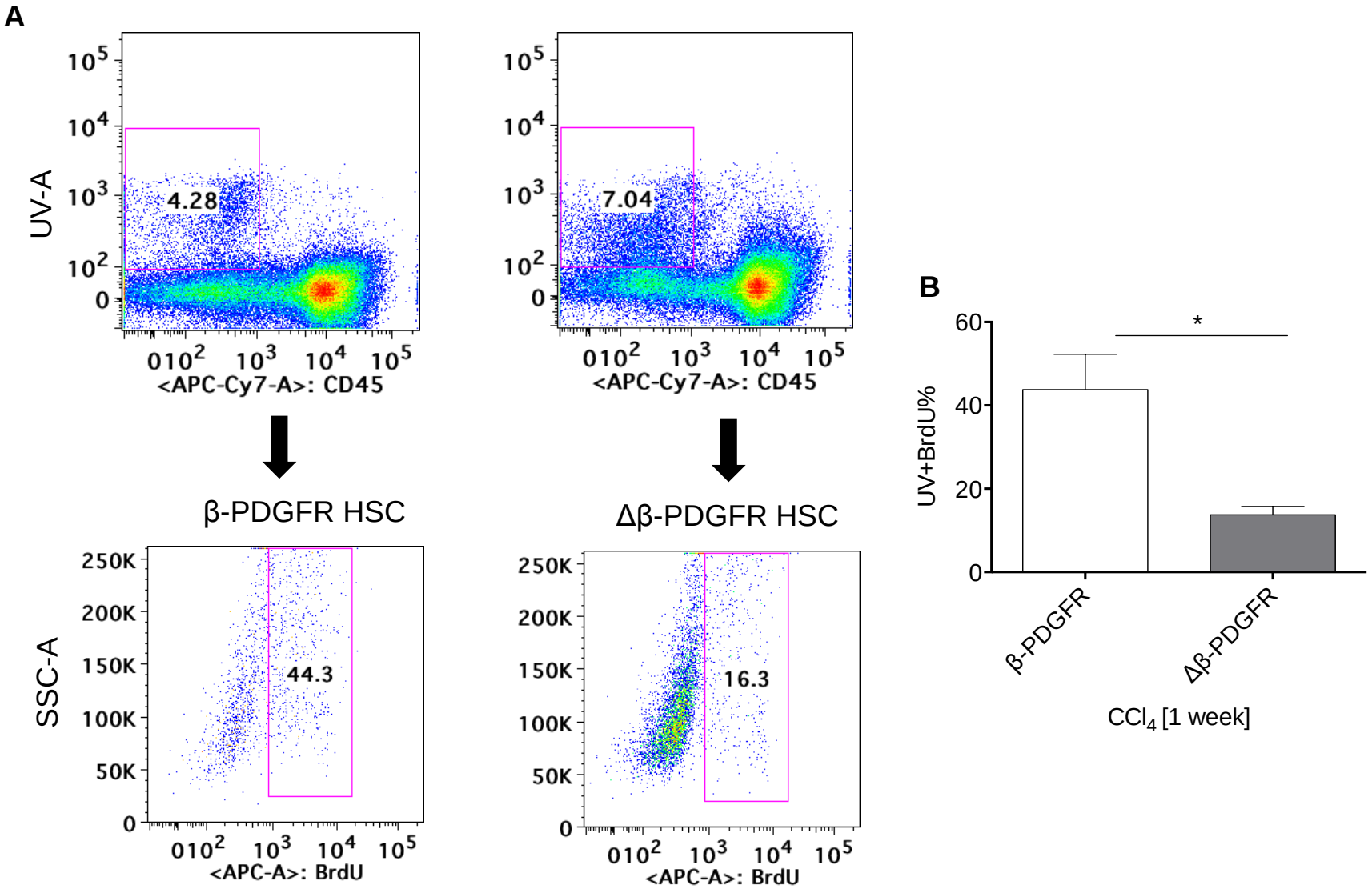

Supplementary figure 7

A

β−PDGFR$^{betaJ/+}$ x Tg(GFAP-Cre)/+
Experimental group (βJ): β-PDGFR$^{+/betaJ}$; Tg(GFAP-Cre)/+
Control group (β-PDGFR): β-PDGFR$^{+/+}$; Tg(GFAP-Cre)/+

B

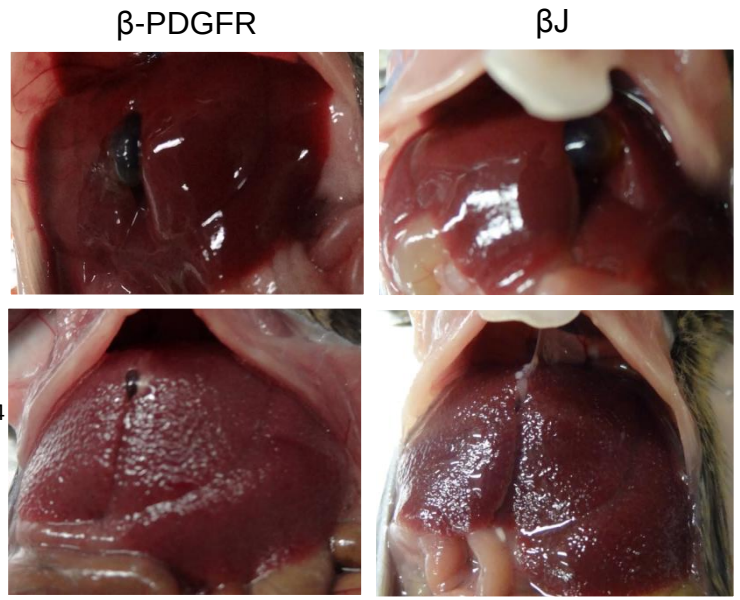

C

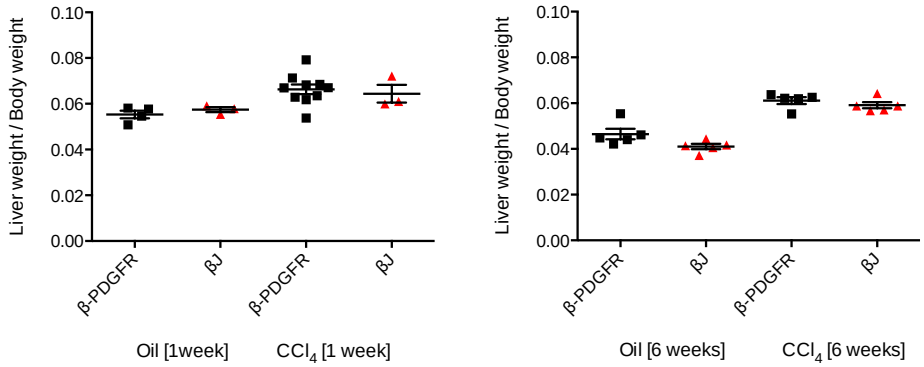

D

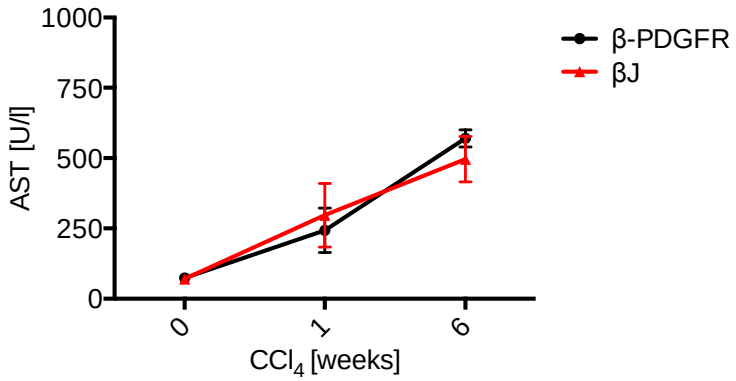

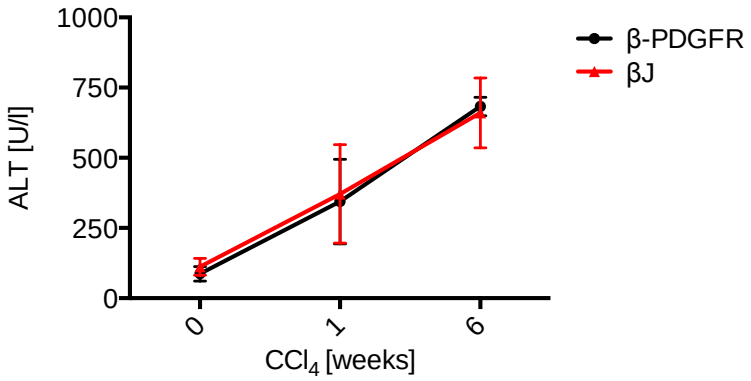

Supplementary figure 8

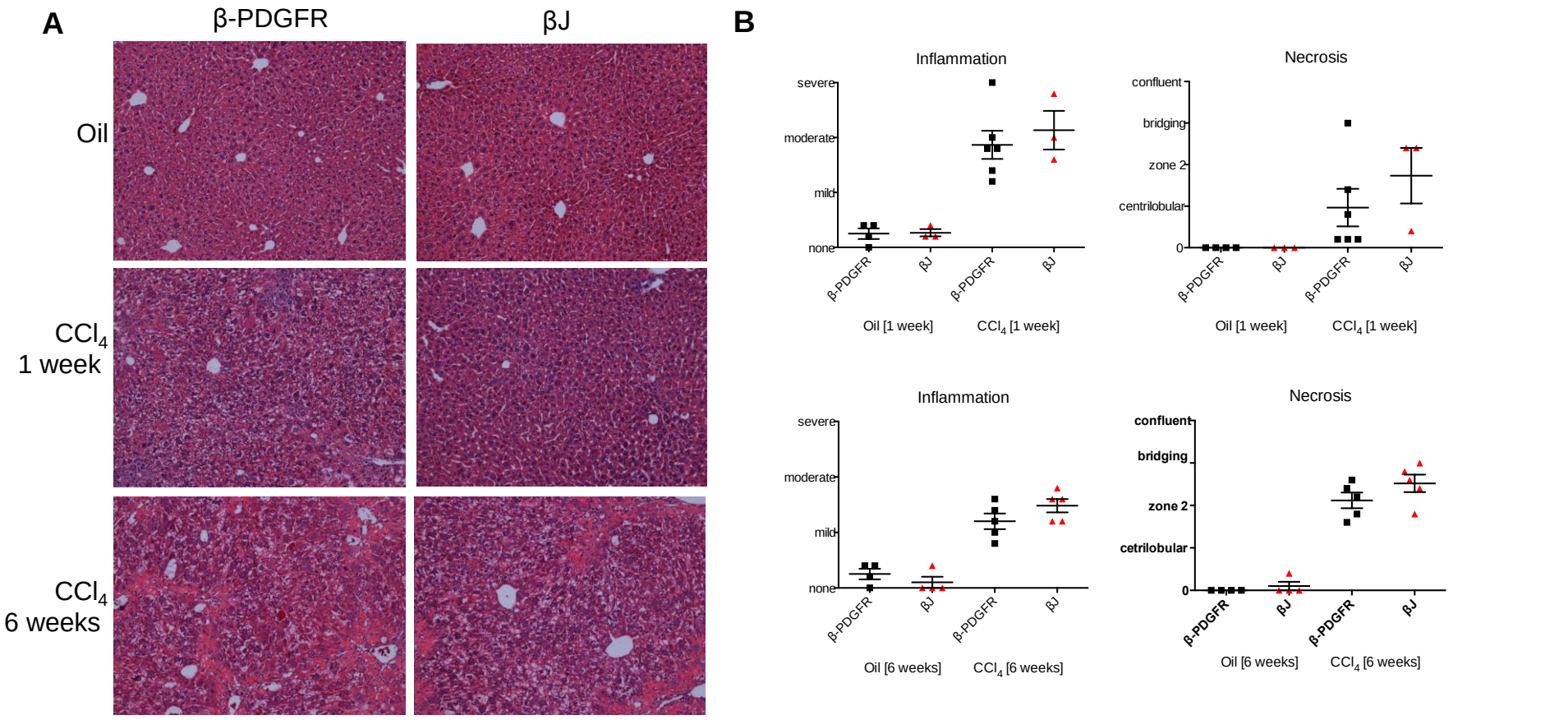

Supplementary figure 9

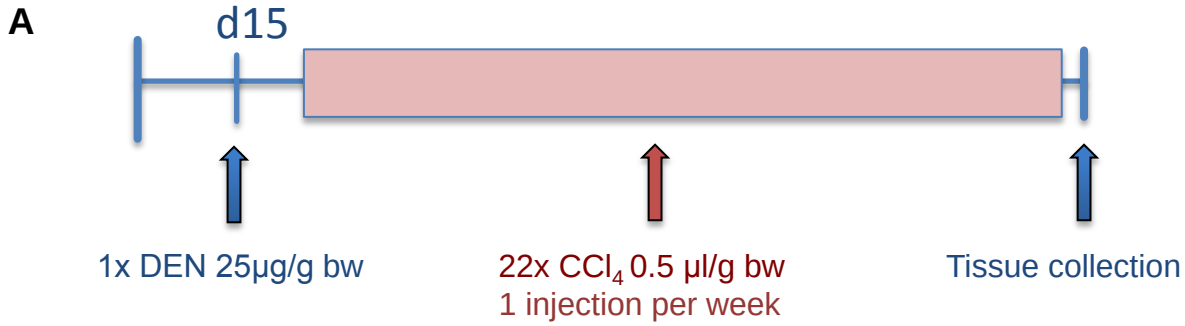

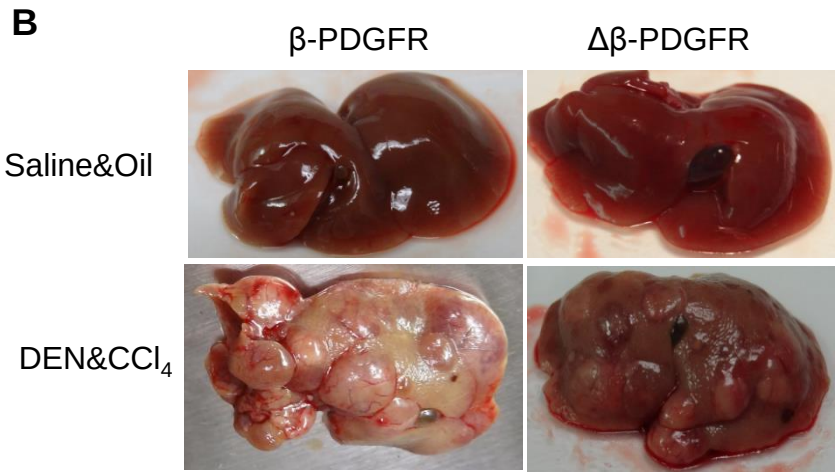

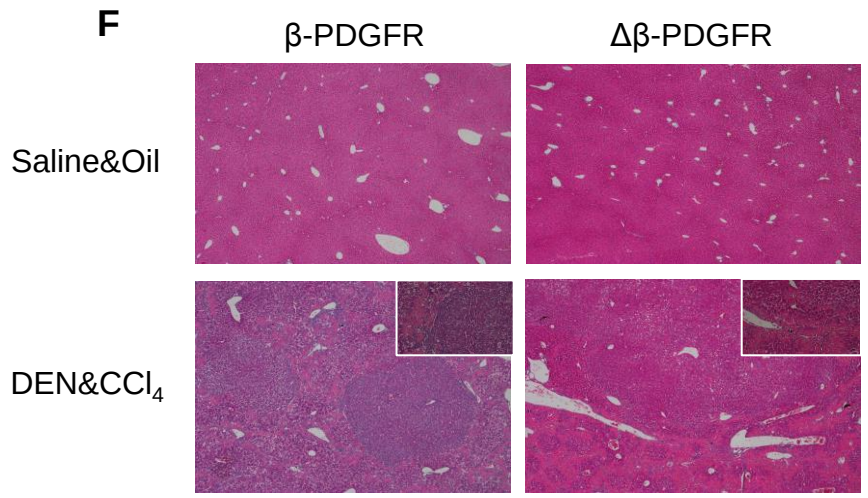

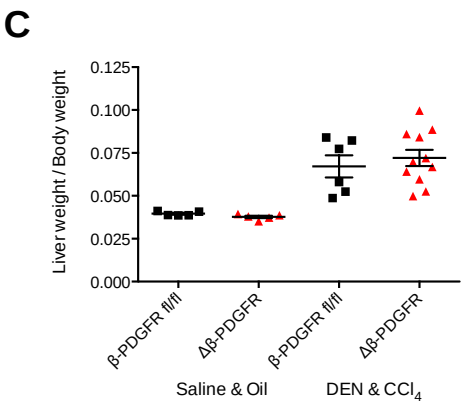

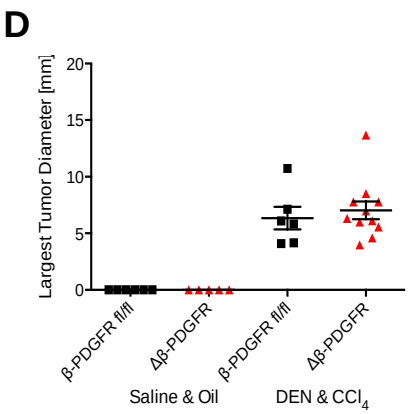

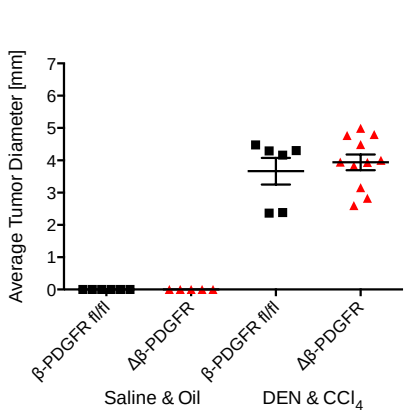

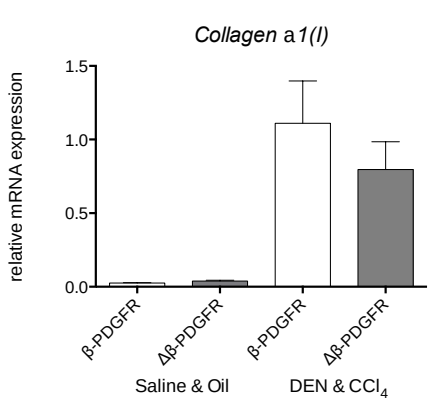

Supplementary figure 10

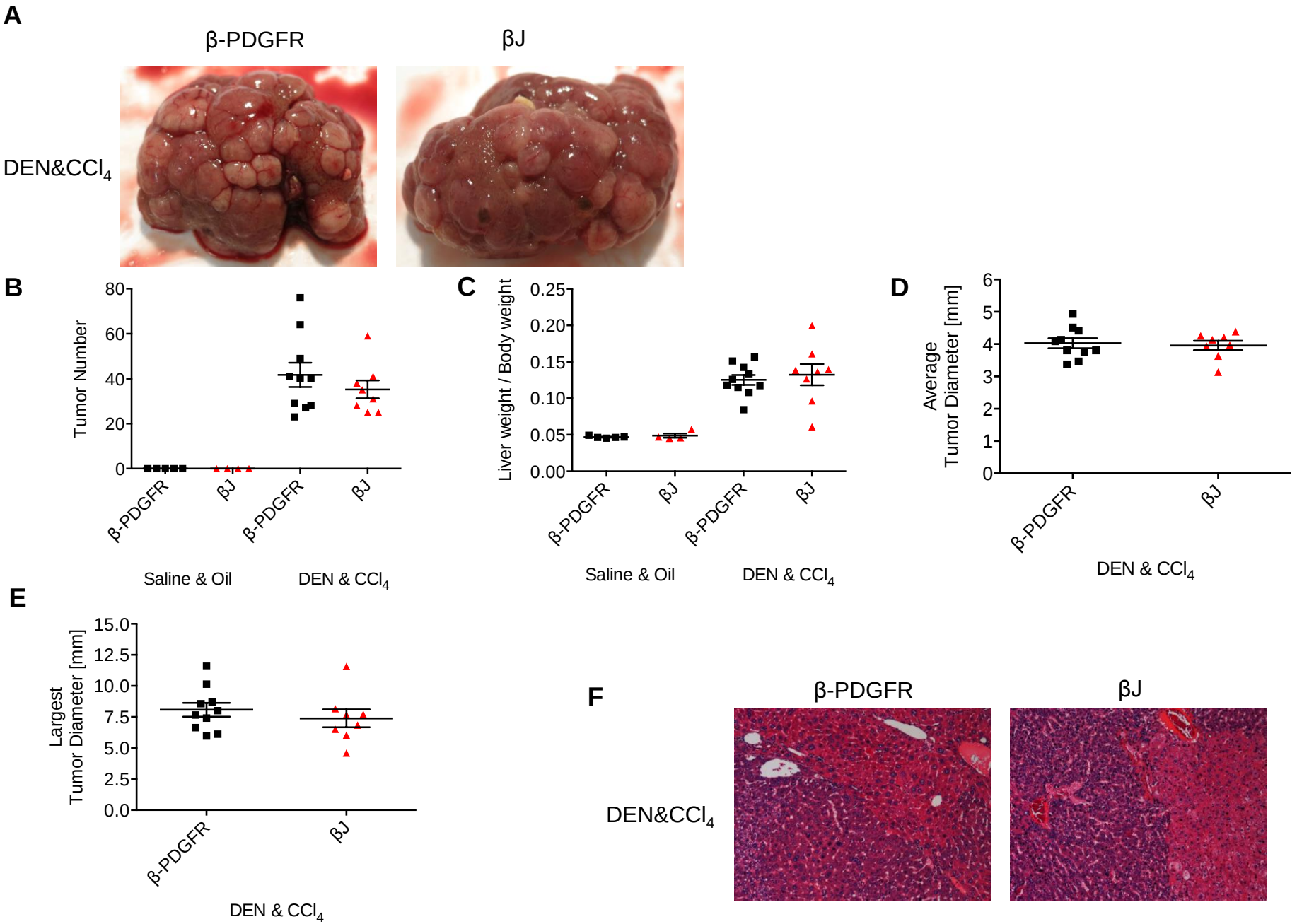

Supplementary figure 11

A

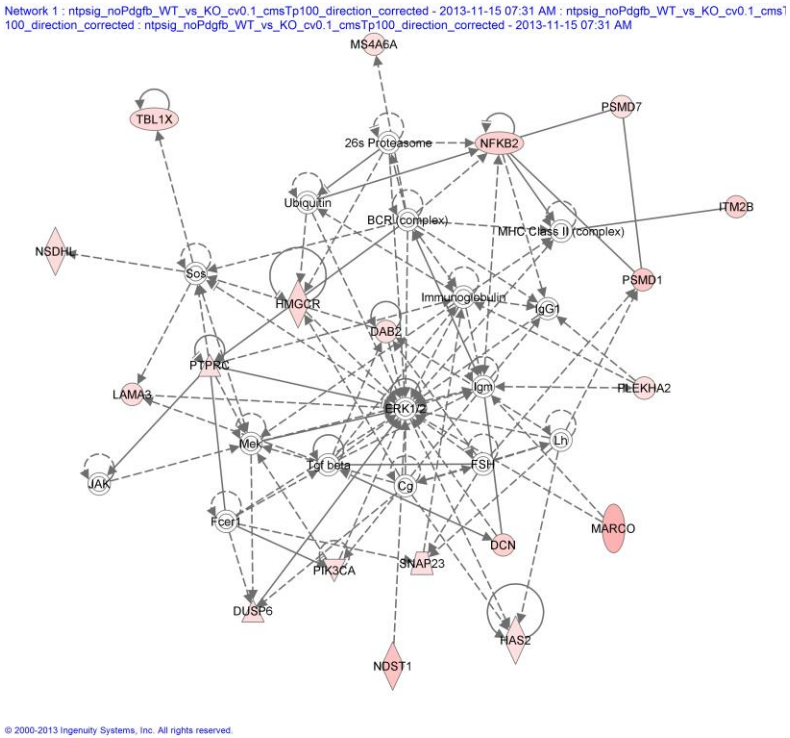

B

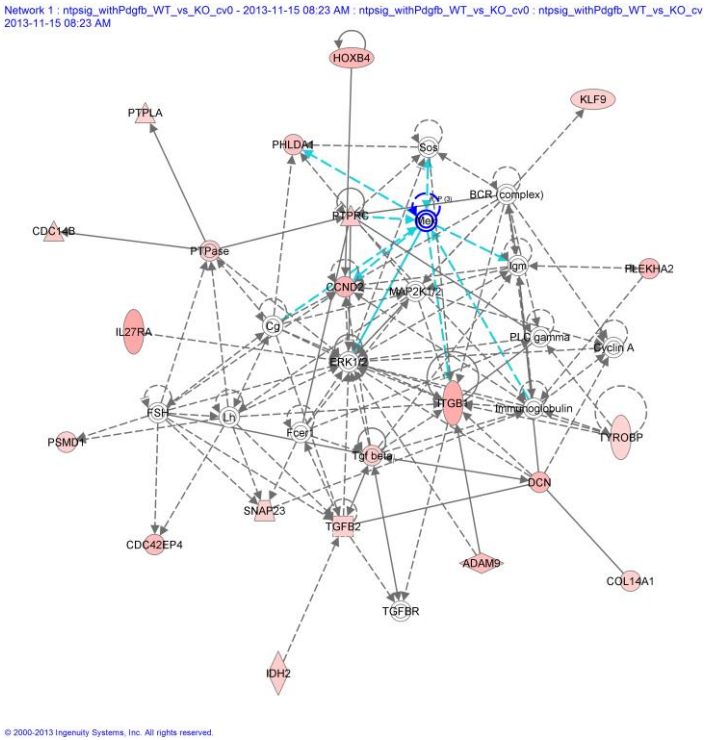

Supplementary figure 12

A

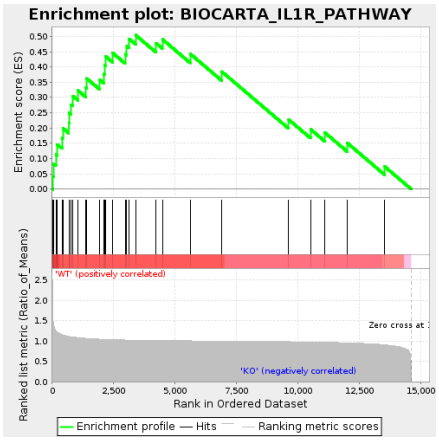

B

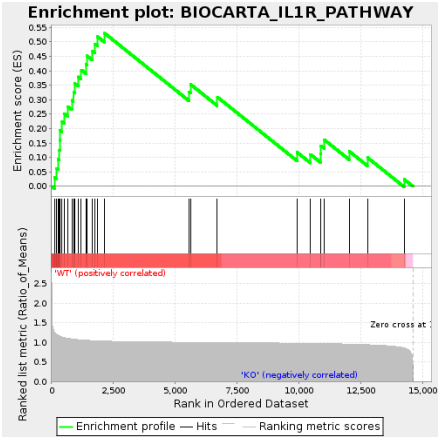

C

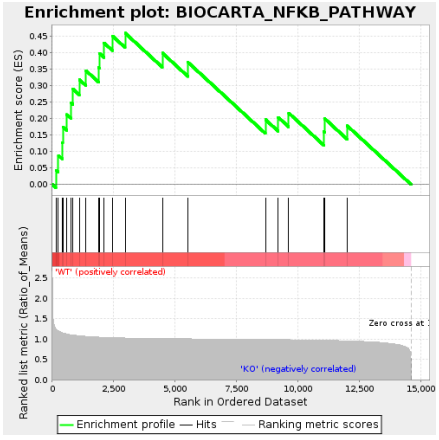

D

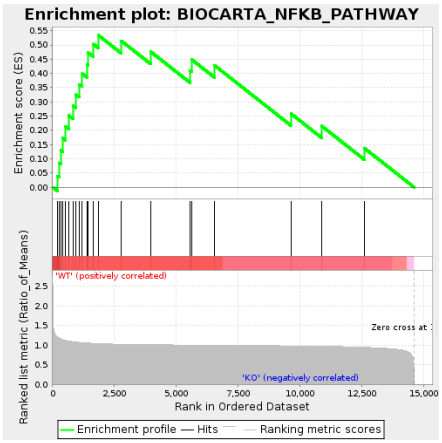

E

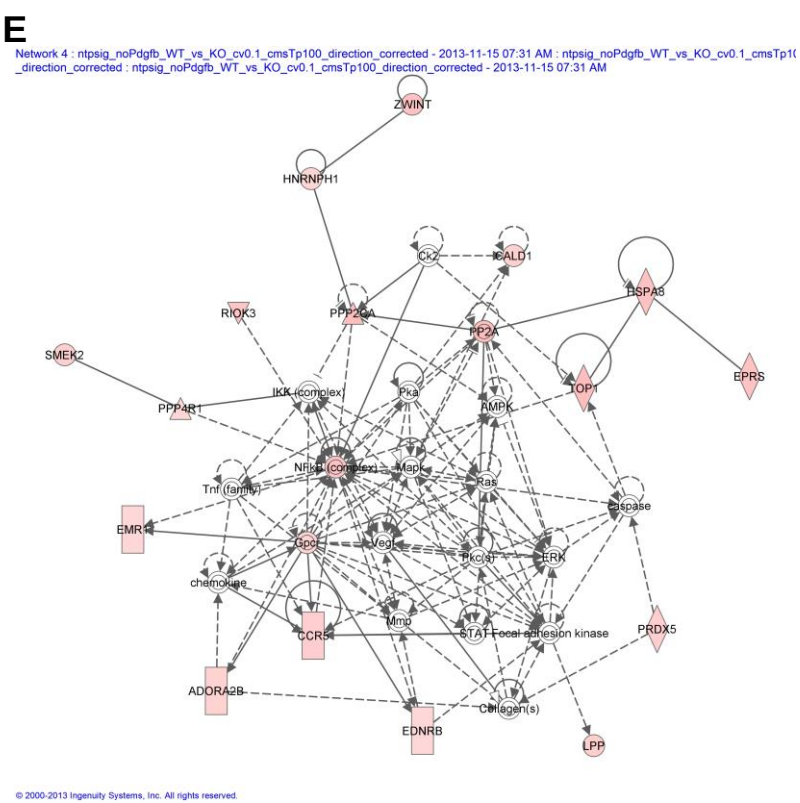

F